This manuscript has been submitted to Elementa: Science of the Anthropocene

Canada's Landfill Methane Inventories: The Challenge of Accurate Modeled and Measurement-Based Emissions

Jordan Stuart (1), Evelise Bourlon (1), Rebecca Martino (1), Lindelwa Coyle (1), Susan Fraser (2), Emil Laurin (2), Felix Vogel (2), Nicholas Bishop (2), Sebastien Ars (2), David Risk (1,*)

(1) FluxLab, Department of Earth and Environmental Sciences, St. Francis Xavier University, Nova Scotia, Canada
(2) Environment and Climate Change Canada, Ontario, Canada

***Corresponding author: David Risk (drisk@stfx.ca)**

Canada's Landfill Methane Inventories: The Challenge of Accurate Modeled and Measurement-Based Emissions

Jordan Stuart[1], Evelise Bourlon[1], Rebecca Martino[1], Lindelwa Coyle[1], Susan Fraser[2], Emil Laurin[2], Felix Vogel[2], Nicholas Bishop[2], Sebastien Ars[2], David Risk[1,*]

[1]FluxLab, Department of Earth and Environmental Sciences, St. Francis Xavier University, Nova Scotia, Canada

[2]Environment and Climate Change Canada, Ontario, Canada

*Corresponding author: David Risk drisk@stfx.ca

Abstract

We present a measurement-based assessment of methane emissions from 42 landfills across diverse climatic regions in Canada. Our findings reveal that emission rates predicted by the First Order Decay (FOD) model used by Environment and Climate Change Canada at the visited sites are substantially higher than most measured emission rates, on average by a factor of 3, particularly for cold and arid climates typical of the Canadian prairie provinces (by a factor of 13 on average). Bias-corrected measurement rates aligned more closely with values reported to the Canadian Greenhouse Gas Reporting Program. Compared to the amounts estimated by the FOD model, our measurement-based estimations show greater variation with changes in climate. At some warmer and wetter sites, measured rates exceeded FOD modeled estimates, underscoring the influence of climate on landfill methane dynamics and FOD model behavior. We also found that measurement-based estimates yield more realistic methane collection effectiveness values than those implied by Canada's FOD-based inventories. Our results suggest that the current FOD inventory model parameters—that include decay rates and oxidation assumptions—should be refined to better reflect site-specific conditions and climate variability across Canada.

Introduction

Like many countries, Canada's waste sector is a major source of methane emissions, emitting an estimated 19 Mt CO_2e in 2023, or 0.51 t CO_2e per capita (Environment and Climate Change Canada, 2025). To track greenhouse gas emissions in the waste sector, Environment and Climate Change Canada (ECCC) compiles Canada's landfill methane inventory using a variation of the Intergovernmental Panel on Climate Change (IPCC) First Order Decay (FOD) waste model with default parameters or national, provincial, or site-level parameters when available (Pipatti and Svardal, 2006). Though this model is used by ECCC to estimate emissions at the provincial level for greenhouse gas reporting in its National Inventory Report of Greenhouse Gas Sources and Sinks in Canada (NIR), it can be configured to estimate site-specific emissions by incorporating available operational information, waste tonnage, waste composition, waste age, decay rate, and methane generation potential. Calculation of methane emission is based on modeled methane generation adjusted for any methane destruction (accounting for flaring efficiency) or utilization and methane oxidation of the generated methane that is not recovered in landfill covers (the IPCC default oxidation factor of 0.1 is used for all regions and years; ECCC, 2025). At municipal solid waste landfills, ECCC (2025; section 7.2.3) estimated the emission uncertainty to be ±76% using the default parameters from the IPCC 2006 Guidelines (IPCC, 2006). Gaps in input activity timeseries are completed with interpolated or extrapolated values (ECCC, 2025).

In addition to compiling Canada's methane inventory, ECCC administers Canada's Greenhouse Gas Reporting Program (GHGRP). Landfills emitting 10 kt CO_2e/year or more are required to report emissions to the GHGRP. However, unlike in the United States, where GHGRP data are integrated into its national inventory estimates (EPA, 2023), Canada uses them to compare and validate its inventory. Canadian landfills reporting to the GHGRP are not required to use a standard methodology. Some operators rely on engineering calculations using the IPCC FOD model or alternatives such as the United States Environmental Protection Agency's LandGEM model.

Differences in methodology contribute to observed discrepancies between operator-reported GHGRP values and the ECCC's IPCC-based estimates. Based on our subset of landfills, the ECCC-modeled emissions are typically higher on a site-by-site basis—sometimes only marginally, but in some cases, more than nine times higher. Such inconsistencies are increasingly problematic because national inventories face government and public scrutiny. Discrepancies between modeled and measured landfill methane emissions are well-documented, with international studies reporting underestimations of up to 200% in individual and governmental inventories (Wang et al., 2024; Scarpelli et al., 2024; Cusworth et al., 2024). In the United States, two recent studies found that measured emissions exceeded American GHGRP-reported values in 47% of cases and were, on average, 2.7 times higher across all American landfills (Scarpelli et al., 2024; Cusworth et al., 2024). In Canada, Thompson et al. (2009) found that the Scholl Canyon model often overestimated methane recovery rates, and LandGEM consistently underestimated them.

The inaccuracy of waste models is due to several factors. Many landfill methane models rely on environmental parameters that are challenging to validate. For example, the moisture content can vary significantly in both space and time due to the heterogeneous nature of landfill waste, which in turn affects the estimation of leachate generation and the amount of anaerobic decomposition. Sampling waste to estimate its moisture often requires heavy equipment and still may not yield representative results (Krause et al., 2023). Also, models often fail to account for seasonal and climatic variability (Gollapalli and Kota, 2018). For example, Scheutz et al. (2011) reported lower-than-expected methane emissions in Denmark due to precipitation patterns, temporal variability, and landfill characteristics. Similarly, Jain et al. (2021) observed lower emissions from landfills in arid regions compared to wetter climates. Among our selected sites, six of the ten most significant differences between ECCC modeled emissions and GHGRP reports are from Alberta and Saskatchewan, regions where annual precipitation may be as low as 250 mm. Effectively mitigating methane depends on accurate inventories so that interventions can be identified and prioritized. In its National Inventory Report (ECCC, 2025), ECCC acknowledges landfill

methane emissions as the largest source of uncertainty at the national level. Landfill methane regulations have been released to reduce waste-sector methane, but the ability to accurately measure the impact of regulations will depend on how well landfill methane emissions and their sources can be quantified. Reducing inventory uncertainty will require improving the quality of the FOD model input data from Canada's approximately 270 large landfills, which account for more than 85% of Canada's methane landfill emissions (ECCC, 2022). Furthermore, improving data collection will enhance model validation capabilities.

Measuring methane emissions comes with several challenges that often stem from temporal changes in weather conditions–particularly fluctuations in barometric pressure and wind speed (Fredenslund et al., 2010; Kissas et al., 2022)–limited site accessibility, complex dispersion patterns caused by wind conditions, topography or obstacles, and the heterogeneous nature of landfill methane sources (Lando et al., 2017; Fjelsted et al., 2019). In rapid screening survey campaigns like the one presented in this study, measurement attempts are not always successful.

This study compares measurement-based landfill methane emission rates with those modeled by ECCC using the IPCC FOD model and those reported to GHGRP. We also examine how climate variability affects measured emissions and their divergence from FOD-modelled emissions, considering factors such as the accumulated waste size, the waste methane potential, and the effectiveness of methane collection systems.

Methods

Site Locations

From July to November 2022, we surveyed landfills across Canada, with or without methane collection systems, varying in size and operational status (open or closed). Surveys were conducted sequentially using two mobile laboratories: one that began in Nova Scotia on Canada's Atlantic coast and moved

westward to Ontario, and another that began in Saskatchewan and continued westward toward British Columbia on Canada's Pacific coast. Most of our measurements were taken on public roads where no permit was required, and safe driving remained the priority. A list of 150 locations was established before the campaign, but weather, instrument issues or inadequate timing prevented us from surveying them all. Unpredictable local weather changes were a factor in reducing the number of landfills visited. We strive to avoid taking measurements immediately after or during weather changes, primarily for fieldwork safety and because rapid changes in barometric pressure have been linked to landfill emission events (barometric pumping; Fredenslund et al, 2010; Xu et al., 2014; Kissas et al., 2022). Taking measurements during a barometric pressure decrease would have led to higher emission estimates, so we favored a more conservative approach. However, we acknowledge that our emission snapshots are biased downward relative to annual emission estimates. For our analysis, we focused on 42 sites (Figure 1), out of 111 surveyed landfills, where we had obtained off-site emission rate estimates under the following conditions: wind speeds within an appropriate range, no weather change, an unobstructed line of sight to the landfill, and no issues with measurement instrumentation.

Measurements

For the landfill emission measurement campaign, we used two mobile survey laboratories. Each mobile laboratory consisted of a Toyota RAV4 outfitted with a Picarro gas analyzer (G2210-i CRDS, Picarro Inc., USA) connected to a high-volume 7 LPM pre-pump. The setup minimized the lag time between the external air inlet and the instrument. At the front of the vehicle, we mounted the air inlet on a mast fixed to the vehicle's roof. An open Y-splitter fitting allowed excess airflow to be released. The mast also housed a 2-axis ultrasonic anemometer (WindSonic, Gill Instruments Ltd, UK), an electric compass (Model 32500, RM Young, USA), and a GPS (18x, Garmin Ltd, USA). All mast-mounted equipment was approximately 2.5 m above ground level. A data logger (CR1000X, Campbell Scientific, USA) recorded all measurements, including internal time, at 2 Hz.

Both gas analyzers were calibrated before the campaign using two gas standards with different CH_4 mixing ratios, prepared by the AmeriFlux Management Program (Lawrence Berkeley National Laboratory, Berkeley, CA, USA) and referenced to within <1 ppb of the World Meteorological Organization CH_4 scale using standards maintained by the U.S. National Oceanic and Atmospheric Administration. We used AmeriFlux standard FB03987 (4.52 ppm CH_4, 516.54 ppm CO_2, prepared August 2019), for which we found an average departure of 0.008 ppm CH_4, and AmeriFlux standard FB04007 (1.81 ppm CH_4, 385.18 ppm CO_2, prepared August 2019), for which the average offset was 5.6×10^{-4} ppm CH_4. Before measuring the standards, the analyzer cavity was purged for several hours with zero–water-vapor gas until H_2O levels stabilized below 0.05%. Both gas analyzers were checked immediately after the campaign using the same procedure to assess drift over the course of the campaign.

During fieldwork, we conducted a second daily check: each morning, we benchmarked each Picarro analyzer with a target gas containing known CO_2 and CH_4 mixing ratios. The cylinder was attached for five minutes to monitor any deviation between the known and measured values. While field benchmarks are inherently more variable than laboratory tests, our field benchmarks were sufficient for detecting major drift, which we did not observe.

Each morning, we also measured the lag time between the inlet and analyzer cavity by introducing CH_4 pulses at the inlet and timing how long it took the pulses to arrive at the analyzer. The measured lag time ensured that the gas mixing ratio measurements with the GPS locations were precisely aligned. To confirm that the slower response time of the Picarro G2210-i adequately captured plumes, we compared our measurements with the measurements of two faster analyzers, a Licor LI7810 and a Picarro G2401, used in a simultaneous companion survey conducted by ECCC. While our Picarro model damped peak CH_4 values and extended plume duration, the areas under the curve were equal between the analyzers (Figures S1 and S2).

We conducted downwind transect measurements across one or multiple plumes, progressing from background levels to peak values and back. We repeated each transect up to 15 times at speeds ranging from 15 to 80 km/h, depending on safety and traffic conditions. When operators granted us landfill access, we also conducted on-site measurements to better characterize potential emission sources. However, in this study, we only used the off-site downwind measurements to estimate emission rates.

Data Processing and Selecting Transects

Following the data quality checks, we calculated true wind vectors using measured wind speeds, compass readings, and GPS data. We calculated the Sun's position and collected meteorological data from the nearest airport that included cloudiness, ceiling height, and wind to estimate atmospheric stability classes using Turner's method (Turner, 1964). We excluded transects collected when wind speeds were less than 1.5 m/s, during highly unstable conditions (Pasquill stability class "A"), or during the night (Pasquill stability classes "E" and "F").

We estimated the ambient methane level using iterative mean suppression (Liland, 2015), and we defined methane enhancements to be the difference between measured and ambient levels. We discarded the transects that had no significant methane enhancement (<0.01 ppm), relative to the instrument precision, noise level, and estimated background variation.

We mapped and assessed the remaining transect locations relative to landfill boundaries. Using Google imagery and Street View, we identified potential obstacles to dispersion (e.g., tall buildings or dense forests) and screened for nearby non-landfill methane sources such as dairy and poultry farms, compost facilities, water treatment plants, cattle exchange centers, and oil and gas infrastructure. We excluded the transects influenced by such obstacles or additional methane sources. Finally, we calculated the distance between each landfill and its associated methane enhancements, retaining only transects where this distance was less than 2.5 km. This 2.5 km distance was selected based on the results of a controlled-release experiment (our approach is identified as Truck A in Hossain et al., 2025), in which emission rates

were largely underestimated at this distance. Because our slow-response gas instrument produced methane enhancements with amplitudes and widths similar to the background methane level, they were barely discernible and were often underestimated during the controlled release experiment.

Estimating Emission Rates

To estimate the landfill emission rates from the measured methane enhancements, we used a Gaussian dispersion model. Gaussian dispersion models are widely used to simulate air pollutant dispersion and have effectively estimated biogas emissions from landfills (Fredenslund et al., 2019; Aronica et al., 2009). While Gaussian methods are somewhat less accurate than tracer gas approaches, they are faster to implement, do not require site access, and cost roughly two-thirds less, making them well-suited for screening studies like ours (Fredenslund et al., 2019; Fallah-Shorshani et al., 2017; Matacchiera et al., 2019).

Many Canadian landfills are in remote areas with limited road networks, often forcing transects to be near landfill fence lines where multiple Gaussian peaks have been observed because several methane sources within a landfill operation are present (Cusworth et al., 2024). In contrast to Fredenslund et al. (2019), we found that it was not always possible to model a completely coalesced plume or to assume the landfill center was the main source of methane. In our case, we did not know the source locations and emission rates. Our approach was like that of Gillespie et al. (2025) and Ars et al. (2020), which involved minimizing differences between the observed enhancements and Gaussian model predictions. Unlike Gillespie's approach, which used either the known centers of emitting features of the landfill or the corners of the landfill as potential emitting sources, we used random sets of potential emitting points sampled from gridded locations within landfill boundaries, and then we simultaneously calculated their emission rates. Both Gillespie's approach and ours were tested concurrently at a controlled methane release site, producing similar rate estimates (Hossain, 2025). The Gaussian model accounted for parameters including source–measurement distances, source and measurement heights above ground,

wind speed, and dispersion coefficients (sigma parameters). We assumed that the corrected wind at the measurement location reflected the wind at the source, and that the source emissions were continuous. We derived the dispersion parameters from the Pasquill-Gifford-Turner model for open-country settings, based on atmospheric stability. Our algorithm estimates the total landfill emission rate by adjusting the contribution from each source to ensure that the sum of modeled methane concentrations matches the measured methane enhancements. More information on the Gaussian Plume Model and the inversion is available in the Supporting Information. We retained only those results for which the total modeled methane enhancement fell between 80% and 200% of the measured enhancement along downwind transects. We calculated the total landfill emission rates by summing the individual source rates. We repeated this operation over 1000 random distributions of sources, and each landfill was attributed the average and standard deviation of the estimated rate ensemble.

Atmospheric conditions, such as wind and stability class, can influence the uncertainties in emission rate estimates. Landfills, due to their topography and heat generation, often create localized microclimates, which means that meteorological parameters measured on nearby roads or at airports might not perfectly represent conditions at the emission sources. We analyzed emissions assuming fixed source heights (4 m above road level) and variable heights from high-resolution digital elevation models (HRDEM; Natural Resources Canada) but found no significant differences in estimated rates. Source height was not a critical parameter when measurements were taken hundreds of meters from the sources.

To evaluate uncertainty and bias, we conducted a controlled release experiment at a closed landfill with a gas collection system (Hossain et al., 2025). This included 35 double-blind tests downwind of eight point sources and two area sources (>200 m^2) spread over 10 ha, emitting 25 kg/h to 250 kg/h. Our method, identified as “Truck A” in the study, consistently captured 66% of true emissions (including both the controlled release and the landfill emissions), with an uncertainty of ±47.6% across rates from 0 kg/h to 238 kg/h (Hossain et al., 2025). When measurements were collected nearly 2.5 km away or with forested obstacles between the landfill and the mobile laboratory, the resulting emission rates of the controlled

release experiment tended to be underestimated. To minimize underestimating the emissions rates in this study, we avoided having distant transects and obstructed lines of sight.

We present the emission rate estimates directly from the Gaussian inversion and as bias-corrected values (adjusted by 1/0.66). Fredenslund et al. (2019) observed a similar downward bias, reporting a factor of 0.72 when they validated a Gaussian model using tracer-gas-correlation results in a study involving 91 landfills across Denmark.

Landfill categories

We categorized landfills by area and climate. For landfill size binning, we divided the 42 landfills into three equal groups—small, medium, and large—based on each site's accumulated waste in place as calculated by ECCC (Figure 2). Our sites span over 5,000 km from Canada's Atlantic coast to its Pacific coast, encompassing climates that range from high-altitude, steppe-like conditions to mild, wet environments. The length of the growing season and the duration of the winter vary greatly from place to place. For climate classification, we initially used Köppen climate zones, but found most landfills clustered within a single zone, in particular, the humid continental zone. To select some of the FOD model parameters, ECCC uses the aridity index, the ratio of precipitation over the potential evapotranspiration (PET), to define two climate zones across Canada: one PET exceeds precipitation (aridity < 1; "dry" climate) and another where PET is lower than precipitation (aridity > 1; "wet" climate). At our selected sites, the aridity and the precipitation are roughly linearly related (Figure S5); the PET do not vary much. To refine the classification, we extracted weather data from local ECCC stations within 50 km of each landfill, including measured daily or hourly precipitation (rain and snow) and measured temperature records from 2018 to 2022. From these data, we calculated annual total precipitation and mean air temperature, averaged over the five past years preceding our measurement campaign. A temperature versus precipitation diagram enabled us to visually cluster the site into five climate categories (see the cluster extents on Figure 2):

- lower precipitation and lower temperature,
- lower precipitation and mid temperature,
- mid precipitation and higher temperature,
- higher precipitation and mid temperature, and
- much higher precipitation and/or much higher temperature.

These categories are relative to our dataset of 42 landfills, for which we defined "much higher" temperature as having an annual mean temperature above 10°C and "much higher" precipitation as over 1750 mm/year; they are only based on the visual inspection of Figure 2, and not based on Canada's or the world's climate zones. More details about the climate clustering are provided in Section S2 of the Supplementary Material. When mapped (Figure 1), the categories revealed meaningful geographic patterns, with wetter climates concentrated along the west and east coasts and colder climates at higher northern latitudes.

Comparing Measurement Estimates with FOD Modeled Values

Unlike the ECCC and GHGRP annual emission estimates, our measurement-based rates represent instantaneous ("snapshot") landfill emissions, primarily during summer (38 sites visited during summer; 6 during fall). Canada's extreme seasonality means summer temperatures can exceed winter values by more than 30°C. The seasonal variability calls into question some of the parameterization of the FOD model. At all sites, ECCC includes a 10% methane oxidation factor on the portion of methane that is not collected to account for methanotrophs in landfill biocovers reducing fugitive methane emissions. This is the default IPCC oxidation value, based on studies by Czepiel et al. (1996a, b) at a New Hampshire landfill. It represents an annual average, with actual oxidation likely negligible in winter but potentially high in summer. Optimal oxidation rates are reported at 25°C to 35°C (Spokas and Bogner, 2011), but methanotrophs can utilize CH_4 at far lower temperatures with an optimal temperature of 3.5°C to 10°C (Omelchenko et al., 1993), and methanotrophic activity has been observed at 1-2°C (Scheutz and

Kjeldsen, 2004; Einola et al., 2007). Chanton et al. (2009, 2011) found annual oxidation fractions ranging from 11% to 89%, with a mean of 35%. Also, Canadian landfills are often capped with thick layers of clay and soil rather than geotextile covers; this operational choice potentially increases oxidation when conditions are favorable. To assess the potential impact of a higher oxidation factor on FOD-modeled emission rates under warm, microbially active summer conditions, we compared measurement-based estimates with the standard ECCC modeled rates (10% oxidation) and with an adjusted model assuming a higher oxidation factor of 35%. This is only for comparison purposes (Figure 5), and we are not suggesting that the oxidation rate is 35% during the summer in Canada. We calculated the adjusted ECCC modeled emission rates by dividing original model estimates by ~1.4 [(1–0.1)/(1–0.35)].

Results

On-site Observations

We gained access to 50% of the sites, which allowed us to better characterize methane sources and identify landfill areas with the highest emissions. Across these sites, the largest emissions were consistently observed at the active working faces, where new waste was deposited daily. These areas typically lacked covers and had not been integrated into landfill gas collection systems, making them major contributors to fugitive methane. Beyond the active working faces, we recorded elevated methane levels around manholes and leachate wells. In some cases, we also detected methane peaks downwind of compost piles during humid weather; however, compost-related methane enhancements were low or absent. Furthermore, we found that operational activities influenced emission patterns. We measured the highest on-site methane mixing ratios during construction activities, such as the installation of landfill gas collection systems, manholes, and leachate wells. These locations frequently produced methane levels high enough to saturate our analyzer (30 ppm). Occasionally, we were on site when leachate wells were being emptied, and at these times, we observed significant methane spikes.

Comparing our Measurement-based Values to ECCC Modeled Values and GHGRP Industry-Reported Values

We obtained ECCC modeled annual methane emission rates for 2022 at 40 of the 42 sites and emission rates for 2021 for 2 landfills. It should be noted that the 2021 modeled rates are based on a slightly different input parameter estimation approach, although they are derived from the same IPCC FOD model. The ECCC 2022 dataset also included annual measured methane flaring and collection amounts from a voluntary survey of landfill operators conducted by ECCC, and estimations of methane generation potential (L_0 in tons of CH_4), especially the accumulated L_0 that accounts for L_0 remaining in the landfill after previous decay. The L_0 represents the potential amount of methane that could be generated from the landfill waste. Of 42 landfills, 31 reported flared and/or utilized methane amounts in 2022. It is unclear whether the sites for which we lack this information do not have a collection system or simply did not report it. We collected industry-reported emission rates for 2022 from the Canadian GHGRP database for 33 of the 42 sites. The measured, modeled, and reported emission estimates are presented in Figure 3. The ECCC rates were consistently the highest of the two types of rates, ranging from near 0 kg/h to 2368 kg/h (mean: 471 kg/h), whereas the GHGRP rates ranged from 36 kg/h to 1511 kg/h (mean: 357 kg/h). With an oxidation rate of 35%, the ECCC rates range from near 0 kg/h to 1710 kg/h, with a mean of 340 kg/h, closer to the GHGRP range. Our direct measurement-based rates were generally lower than the ECCC or GHGRP rates, ranging from 3 kg/h to 511 kg/h with a mean of 118 kg/h. When we applied the bias correction from the controlled release experiment, our adjusted rates ranged from 5 kg/h to 774 kg/h (mean: 179 kg/h).

The GHGRP and ECCC rate distributions had a primary mode at 178 kg/h, whereas the measurement-based rate distribution peaked at 30 kg/h (Figure 4). However, the bias-corrected measurement-based distribution and GHGRP distribution shared a secondary mode from around 690 kg/h to 750 kg/h.

The ECCC emission rates exceeded 39 direct measurement-based rates and 37 bias-corrected measurement-based rates out of 42 sites (resp. 93% and 88%) and were higher than the GHGRP-reported rates for 20 of 33 sites (61%). In contrast, direct measurement-based rates surpassed GHGRP-reported values for only 4 of 33 sites (12%), and bias-corrected rates exceeded GHGRP values for 9 of 33 sites (27%). The five sites where our bias-corrected estimated rates exceeded the ECCC modeled rates are all in wet climate categories. Of the five, two have similar rates, with a difference of less than 10kg/h. For the three other sites, the ECCC modeled rates are also lower than the GHGRP rates.

We found that the highest emission rates were from open landfills. Of the 42 sites we visited, 9.5% (4 sites) were closed; that is, they no longer accepted waste and had completed final covers and landscaping. Some of these closed sites had been repurposed for recreational use (e.g., golf courses, dog parks). At closed sites, we observed relatively low bias-corrected emission rates (11 kg/h to 244 kg/h), which were close to ECCC FOD estimates (near 0 kg/h to 257 kg/h). However, for two of three closed sites, operators reported unusually high values to the GHGRP (449 kg/h and 779 kg/h), exceeding our measurement-based and the ECCC modeled estimates.

For subsequent analyses, we focused on the bias-corrected values because they compared more favorably to “true” emissions (i.e., the true release rates of the controlled release experiment by Hossain et al. (2025)) on the measurement days without altering patterns relative to the ECCC modeled or GHGRP values. On average, the ratio of the ECCC rates to the measurement-based rates was 3.3 for closed sites (mean difference: 57 kg/h) and 6.4 for open sites (mean difference: 317 kg/h). Overall, the bias-corrected measurement-based rates range compares better with the GHGRP range ($R^2 = 0.636$, slope = 0.529) than with the ECCC FOD range ($R^2 = 0.627$, slope = 0.335) (Figure 5). Adjusting the ECCC FOD estimates for 35% oxidation improved the comparison with our measurement-based rates ($R^2 = 0.627$, slope = 0.463; Figure 5). However, when their respective uncertainties are accounted (76% for ECCC and 47.6% for measurement-based estimates), ECCC and measurement-based emission rate estimate ranges overlap, except for a few landfills located in the drier areas of our study.

It should be noted that our measurements assessed only the emitted methane, not the methane produced (the sum of the methane emitted, collected, and oxidized). Landfill operators report the amount of methane flared and/or utilized to ECCC, but we do not know the amount of microbially oxidized methane. Therefore, we calculated methane collection *effectiveness* (collected / emitted+collected) instead of collection efficiency (collected/produced). Lower measurement-based rates resulted in higher calculated collection effectiveness, with a median of 51% overall and 76% for the large landfills, consistent with engineering expectations for systems installed on covered landfill areas. In contrast, we found the collection effectiveness derived from the ECCC FOD estimates to be substantially lower, with a median of 20% overall and 52% for the large landfills (Figure 6). The greater efficiency observed at the largest sites (in terms of accumulated waste) may be attributed to their higher collection system coverage, as they have a larger ratio of closed cell area to active cell area compared to smaller sites. Figure 7 shows the distribution of effectiveness for two types of climates: "dry", which combines the two lower precipitation categories, and "wet", which comprises the mid, high, and higher precipitation climate categories. The measurement-based emission rates do not lead to any difference in effectiveness, with a similar range and the same median. However, the ECCC emission estimates suggest a large difference in effectiveness, with a lower effectiveness at "dry" sites than at "wet" sites.

As shown in Figure 8, relative to measurement-based rates, the ECCC underpredicts emissions in the warmest, wettest areas (the west coast). However, in drier climates, particularly in Canada's arid central regions, the measurement-based rates diverged sharply from the ECCC FOD estimates, which are on average more than12 times higher than the measured rates, likely because the model does not sufficiently account for the reduction of anaerobic waste degradation due to waste dryness.

Discussion

The key finding of this study is that measurement-based summer snapshots of methane emissions at Canadian landfills are on average lower than the annual emissions predicted by the ECCC FOD modeled

emissions. When expressed as percentages, the measurement-based emission rates are, on average, 77%, 70%, 56% and 38% lower for the climate categories of lower precipitation and lower temperature, lower precipitation and mid temperature, mid precipitation and higher temperature and higher precipitation and mid temperature, respectively. The difference is -52% for the "much higher precipitation and/or much higher temperature" category. This divergence reflects a combination of factors: potential bias in the measurement technique, unrealistic model parameters, or both. Our rates were derived from field surveys conducted primarily during the summer with warm air temperatures and low wind speeds. Barometric pressure and temperature were measured at only a few landfills where sensor towers could be deployed, so these sparse records do not allow us to conclude anything about the influence of atmospheric pressure or temperature. In their 2025 study, Gillespie et al. examined how these drivers could affect measurement-based emission estimates at landfills in Ontario. They found that inclusion of these drivers improves the slope of the best-fit line compared to inventoried emissions, though it does not significantly alter the correlation coefficients. However, methane oxidation by landfill cover layers could be more effective during summer, when our surveys were conducted, than during winter, and could be higher than the 10% default annual oxidation factor assumed in the ECCC FOD modeling. Methanotroph activity depends on landfill cover characteristics and increases with temperature (Börjesson and Svensson, 1997; Park et al., 2005). Although cover properties vary among landfills and with environmental conditions, oxidation can be a significant factor in the differences between our measurement-based rates and ECCC FOD estimates, underscoring the importance of methanotrophs and covers in reducing landfill emissions.

This study also highlights the limitations of applying default or large-scale model parameters, especially decay rates (k), across Canada's diverse climate zones to model the methane generation at each landfill. Our measurement-based estimates were substantially variable depending on the climate zone. Figure 9 illustrates methane generation (emitted + 10% oxidized + recovered) per accumulated methane generation potential L_0 for each climate category. The CH_4 generation potential L_0 (in tonnes of CH_4) is estimated from the mass of degradable organic matter multiplied by the fraction of landfill gas that is CH_4 (1/2) and

386 the molecular weight ratio of CH_4 over C (16/12). Note that this L_0 definition is different from the one
387 provided in the IPCC 2000 Good Practice Guidance, where it is expressed as tonnes of methane per
388 tonnes of waste landfilled. The accumulated methane generation potential L_0 accounts for the previous
389 year's L_0 decay. In the ECCC modeling, the amount of degradable organic matter is based on waste
390 composition determined at the provincial level, not the site level, and does not account for any site-
391 specific variability. As a result, ECCC might overestimate methane production at large urban landfills
392 where organic waste diversion programs are active. Figure 9 illustrates the contrast between
393 measurement-based methane generation per methane generation potential L_0, which increases as the
394 climate gets wetter and warmer, and the ECCC FOD-based methane generation, which displays bimodal
395 variability—showing a similar amount at all the drier sites and a different, consistent amount at all the
396 wetter sites. The measurement-based methane generation is lower than the model-based values except for
397 the wettest climate zone. This could be an indication of a potential overestimation of the methane
398 generation, hence the methane emission, especially in low precipitation areas. There is no clear
399 relationship with the amount of landfill waste.

400 Assuming a methane generation time of 15 years followed by negligible generations, the measurement-
401 based methane generation translates to a methane generation potential from the measurement-based rates
402 of 1 m^3 to 56 m^3 CH_4 per tonne of total accumulated waste (the annual total amount of waste that remains
403 after some water removal and decomposition), and 27 m^3 and 33 m^3 CH_4 per tonne of accumulated waste
404 from ECCC FOD modeled methane generation for "dry" and "wet" climate respectively. In a review by
405 Krause et al. (2016), methane generation potentials ranged from 20 m^3 to 223 m^3 CH_4 per tonne of
406 municipal solid waste. Our values and ECCC values fall within the lower quarter of this range, which we
407 expect for dry and cold Canadian conditions. However, ECCC values are higher than measurement-based
408 values for all but the wettest and/or warmest sites.

409 The ECCC FOD estimates have a pronounced upward bias for cold and arid climates and underestimate
410 emissions for the warmer and/or wetter areas (Figure 8). Vu et al. (2017) demonstrated that FOD models

411 with default parameters fail to capture methane production dynamics for cold semi-arid climates, with
412 mean percentage errors ranging from 55% to 135%. We estimated the bulk landfill waste decay rates (k)
413 both from our measurements, assuming a 10% methane oxidation, and the FOD-modeled rates, as:

$$k = -\ln\left(1 - \frac{emitted + collected + oxidized}{L_0}\right). \quad (1)$$

414 The values are reported in Table A. Decay rates vary widely by waste composition and moisture content,
415 and nutrient availability, pH, and temperature are less significant factors. Our median k values vary from
416 0.004 to 0.0063 y^{-1}, from the coldest, driest sites to the warmest, wettest sites. The FOD-based k values,
417 accounting for regional waste composition, are 0.03 y^{-1} for the dry sites and 0.05 y^{-1} for the wet sites. The
418 values range within the range reported by Jain et al. (2021) from a study of 114 landfills in the United
419 States, from 0.004 to 0.226 y^{-1}, with a median of 0.068 y^{-1}. Both Canadian FOD and measurement-based k
420 values fall within the lower half of the US k value range. This may be due to factors such as lower
421 temperatures, prolonged sub-zero periods, reduced precipitation, and differences in waste composition
422 resulting from distinct organic diversion practices. The measurement-based k values indicate that waste
423 decay is significantly slower under dry and cold conditions than assumed by the FOD model. This
424 disparity may be further amplified because our measurements were taken during the summer, which can
425 be drier than other seasons and may affect waste moisture levels. The default IPCC bulk waste decay rate
426 values—0.05 y^{-1} for boreal/temperate dry climates and 0.09 y^{-1} for boreal/temperate wet climates—are,
427 on average, 1.7 times higher than the ECCC FOD values and over 3 times higher than the measurement-
428 based estimates. More accurate decay rates and methane generation potentials tailored to Canadian
429 climate zones could improve inventory estimates and scale them downward. Given Canada's rapidly
430 changing climate, understanding methane generation under different environmental conditions is critical.

431 Our findings emphasize the need for models to reflect the landfill dynamics associated with site
432 specificity in each region to accurately assess gas collection system performance. Based on our
433 measurement-based emission rates, the median collection effectiveness was 51%, aligning with studies by

Duan et al. (2022), who reported a range of 13% to 86% and a mean of 50% at Danish landfills using the same effectiveness definition (i.e., no oxidation accounted). In contrast, the ECCC FOD model estimates suggested an average collection effectiveness of only 20%, implying that collection systems were far less effective than they were in practice.

Extrapolating annual emissions from single-day measurements introduces uncertainty due to diurnal and seasonal variability in landfill emissions. However, models also require credible annual parameters that reflect landfill management and climate. Repeated measurements over multiple days, seasons, and years would improve accuracy and confidence. Our research contributes to a growing body of work informing inventory refinement and demonstrates the value of measurement-based approaches in optimizing model parameters and reducing uncertainty. Improving inventory data collection from landfill operations and waste composition would further reduce uncertainty and support evidence-based policy development.

Canada's regulatory plan (Government of Canada, 2024) aims to reduce landfill methane emissions by 50% below 2019 levels by 2030, through a new regulated framework based on surface methane concentration thresholds. Methane mitigation measures include the implementation or expansion of landfill methane control approaches such as landfill gas recovery systems, engineered biosystems, or methane flaring. Currently, about 150 large landfills in Canada have gas recovery systems, and expanding their installation at more sites could be a significant step. However, engineering calculations often assume 75% and 90% collection efficiency for open and closed sites, respectively, which are much higher than the one estimated from both measurements and FOD modeling (a median efficiency of 51% and 20%, respectively). We hypothesize that active working face emissions, which can account for up to half the total landfill emissions and typically lack collection infrastructure (Scarpelli et al., 2024; Risk et al., 2025), might be overlooked. Because of lower efficiency, collection systems might need to be deployed at a larger number of sites than planned. To achieve the expected gas collection efficiency, it is important that strategies address emissions from active working faces, particularly when those areas represent a significant portion of the total landfill area. While only a few landfills in Canada currently use active face

collection systems, the technology is widely deployed in countries like the United Kingdom and could be scaled for use in Canada.

On a positive note, our measurements suggest that landfill methane emissions in the Canadian inventory tend to be overestimated. Emissions from arid regions were notably overpredicted. Our bias-corrected measurements, while offering a snapshot at a limited number of Canadian landfills, indicated that landfill methane inventories could be overstated by at least a factor of two, given the distribution of landfills across Canada.

The Canadian government has already demonstrated a commitment to inventory accuracy by implementing a measurement-informed methane inventory for the oil and gas sector—the first of its kind globally—by incorporating extensive aircraft site measurements annually to verify inventory estimates. A similar approach could be applied to the waste sector, where fewer sites and highly accurate methods, such as the ground-based tracer gas method, could make the initiative feasible and impactful.

Conclusion

This study provided a measurement-based assessment of methane emissions from Canadian landfills on a national scale, revealing systematic discrepancies between ECCC estimates based on the IPCC FOD model and the measurement-based estimates. Our findings showed that the ECCC modeling often overestimates emissions from cold and arid regions, while occasionally underestimating emissions from warmer, wetter climates. These mismatches highlight the need to refine inventory parameters, such as decay rates and oxidation assumptions, to better reflect Canada's climate diversity and site-specific landfill practices.

By integrating bias-corrected mobile survey measurements with inventory data, we demonstrated that Canada's landfill methane inventory might be overstated—potentially by a factor of two. This suggests that methane mitigation targets could be more achievable than anticipated, especially if active work faces

and other high-emitting sources were effectively managed. However, improving inventory accuracy requires measurement campaigns, not necessarily similar to the survey approach used in this exploratory study, at a selection of sites that reflect all the landscape and climatic conditions encountered in Canada, and better inventory data collection on landfill operations and waste composition to improve the input parameters of FOD models. Tracking emissions over an extended period at certain sites would provide valuable insights into how factors such as weather and operational changes affect emission variability. As Canada moves towards ambitious waste sector methane reduction targets, aligning mitigation strategies with measurement-informed inventories will be critical to success. Our study underscores how valuable empirical data can be for validating models and supporting the case for scaling up measurement-informed approaches—already pioneered in Canada's oil and gas sector—to achieve similar transparency and effectiveness in waste management.

References

Aronica, S, Bonanno, A, Piazza, V, Pignato, L, Trapani, S. 2009. Estimation of biogas produced by the landfill of Palermo, applying a Gaussian model. *Waste Management* 29(1): 233–239. https://doi.org/10.1016/j.wasman.2008.02.026

Ars, S, Vogel, F, Arrowsmith, C, Heerah, S, Knuckey, E, Lavoie, J, Lee, C, Pak, NM, Phillips, JL, Wunch, D. 2020. Investigation of the Spatial Distribution of Methane Sources in the Greater Toronto Area Using Mobile Gas Monitoring Systems. *Environmental Science and Technology* 54(24): 15671–15679. https://doi.org/10.1021/acs.est.0c05386

Börjesson, G, Svensson, BH. 1997. Seasonal and diurnal methane emissions from a landfill and their regulation by methane oxidation. *Waste Management and Research* 15(1): 33–54. https://doi.org/10.1006/wmre.1996.0063

Chanton, JP, Powelson, DK, Green, RB. 2009. Methane Oxidation in Landfill Cover Soils, is a 10% Default Value Reasonable? *Journal of Environmental Quality* 38(2): 654–663. https://doi.org/10.2134/jeq2008.0221

Chanton, J, Abichou, T, Langford, C, Spokas, K, Hater, G, Green, R, Goldsmith, D, Barlaz, MA. 2011. Observations on the methane oxidation capacity of landfill soils. *Waste Management* 31(5): 914–925. https://doi.org/10.1016/j.wasman.2010.08.028

Cusworth, DH, Duren, RM., Ayasse, AK, Jiorle, R, Howell, K, Aubrey, A, Green, RO, Eastwood, ML, Chapman, JW, Thorpe, AK, Heckler, J, Asner, GP, Smith, ML, Thoma, E, Krause, MJ, Heins, D, Thorneloe, S. 2024. Quantifying methane emissions from United States landfills. *Science* 383(6690): 1499–1504. https://doi.org/10.1126/science.adi7735

Czepiel, P. M., Mosher, B., Crill, P. M., & Harriss, R. C. (1996a). Quantifying the effect of oxidation on landfill methane emissions. *Journal of Geophysical Research: Atmospheres*, *101*(D11), 16721–16729. https://doi.org/10.1029/96JD00222

Czepiel, P. M., Mosher, B., Harriss, R. C., Shorter, J. H., McManus, J. B., Kolb, C. E., Allwine, E., & Lamb, B. K. (1996b). Landfill methane emissions measured by enclosure and atmospheric tracer methods. *Journal of Geophysical Research: Atmospheres*, *101*(D11), 16711–16719. https://doi.org/10.1029/96JD00864

Duan, Z, Kjeldsen P, Scheutz, C. 2022. Efficiency of gas collection systems at Danish landfills and implications for regulations. *Waste Management* 139: 269–278. https://doi.org/10.1016/j.wasman.2021.12.023

Einola, J.-K. M., Kettunen, R. H., & Rintala, J. A. (2007). Responses of methane oxidation to temperature and water content in cover soil of a boreal landfill. *Soil Biology and Biochemistry*, *39*(5), 1156–1164. https://doi.org/10.1016/j.soilbio.2006.12.022

Environment and Climate Change Canada. 2022. Reducing methane emissions from Canada's municipal solid waste landfills: Discussion paper. https://www.canada.ca/en/environment-climate-change/services/canadian-environmental-protection-act-registry/reducing-methane-emissions-canada-municipal-solid-waste-landfills-discussion.html

Environment and Climate Change Canada. 2025. National Inventory Report 1990–2023: Greenhouse Gas Sources and Sinks in Canada. Available online at: canada.ca/ghg-inventory.

EPA (2023) Inventory of U.S. Greenhouse Gas Emissions and Sinks: 1990-2021. U.S. Environmental Protection Agency, EPA 430-R-23-002. https://www.epa.gov/ghgemissions/inventory-us-greenhouse-gas-emissions-andsinks-1990-2021.

Fallah-Shorshani, M, Shekarrizfard, M, Hatzopoulou, M. 2017. Integrating a street-canyon model with a regional Gaussian dispersion model for improved characterisation of near-road air pollution. *Atmospheric Environment* 153: 21–31. https://doi.org/10.1016/j.atmosenv.2017.01.006

Fjelsted, L., Christensen, A. G., Larsen, J. E., Kjeldsen, P., & Scheutz, C. (2019). Assessment of a landfill methane emission screening method using an unmanned aerial vehicle mounted thermal infrared camera – A field study. Waste Management, 87, 893–904. https://doi.org/10.1016/j.wasman.2018.05.031

Fougère, CR, Ghasemi, D, Khaleghi, A, Coyle, L, Bourlon, E, Li, H, Smith, M, Risk, D. 2025. Estimating Canadian landfill methane emissions from aircraft measurements [preprint]. Social Science Research Network. https://doi.org/10.2139/ssrn.5186900

Fredenslund, AM, Mønster, J, Kjeldsen, P, Scheutz, C. 2019. Development and implementation of a screening method to categorise the greenhouse gas mitigation potential of 91 landfills. *Waste Management* 87: 915–923. https://doi.org/10.1016/j.wasman.2018.03.005

Gillespie, LD, Ars, S, Alkadri, S, Urya, S, Khoo, T, Fraser, S, Vogel, F, Wunch, D. 2025. Estimating methane emissions from the waste sector in Southern Ontario using atmospheric measurements. *Journal of the Air and Waste Management Association* 75(2): 144–163. https://doi.org/10.1080/10962247.2024.2435340

Gollapalli, M, Kota, SH. 2018. Methane emissions from a landfill in north-east India: Performance of various landfill gas emission models. *Environmental Pollution* 234, 174–180. https://doi.org/10.1016/j.envpol.2017.11.064

Government of Canada. 2024. *Canada Gazette, Part 1, Volume 158, Number 26: Regulations Respecting the Reduction in the Release of Methane (Waste Sector)*. Government of Canada, Public Works and

559 Government Services Canada, Integrated Services Branch, Canada Gazette. https://gazette.gc.ca/rp-
560 pr/p1/2024/2024-06-29/html/reg5-eng.html

561 Hossain, RI, Buntov, P, Dudak, Y, Martino, R, Fougere, C, Naseridoust, S, Bourlon, E, Lavoie, M,
562 Khaleghi, A, Hall, C, Risk, D. 2025. A controlled release experiment for investigating methane
563 measurement performance at landfills [preprint]. Earth ArXiv.
564 https://eartharxiv.org/repository/view/8985/

565 (IPCC) Intergovernmental Panel on Climate Change. 2006. 2006 IPCC Guidelines for National
566 Greenhouse Gas Inventories, Volume 4: Agriculture, Forestry and Other Land Use. IPCC National
567 Greenhouse Gas Inventories Programme. Eggleston HS, Buendia L, Miwa K, Ngara T, Tanabe K
568 (eds). Hayama

569 IPCC. 2000. Good Practice Guidance and Uncertainty Management in National Greenhouse Gas
570 Inventories - J Penman, D Kruger, I Galbally, T Hiraishi, B Nyenzi, S Emmanul, L Buendia, R
571 Hoppaus, T Martinsen, J Meijer, K Miwa and K Tanabe (Eds). ISBN 4-88788-000-6.
572 https://www.ipcc.ch/publication/good-practice-guidance-and-uncertainty-management-in-national-
573 greenhouse-gas-inventories/

574 Jain, P, Wally, J, Townsend, TG, Krause, M, Tolaymat, T. 2021. Greenhouse gas reporting data improves
575 understanding of regional climate impact on landfill methane production and collection. *PLoS One*
576 16(2): e0246334. https://doi.org/10.1371/journal.pone.0246334

577 Kissas, K., Ibrom, A., Kjeldsen, P., & Scheutz, C. (2022). Methane emission dynamics from a Danish
578 landfill: The effect of changes in barometric pressure. *Waste Management*, *138*, 234–242.
579 https://doi.org/10.1016/j.wasman.2021.11.043

Krause, MJ, Chickering, GW, Townsend, GT, Reinhart, DR. 2016. Critical review of the methane generation potential of municipal solid waste. *Critical Reviews in Environmental Science and Technology* 46(13): 1117–1182. https://doi.org/10.1080/10643389.2016.1204812

J. Krause, M., Eades, W., Detwiler, N., Marro, D., Schwarber, A., & Tolaymat, T. (2023). Assessing moisture contributions from precipitation, waste, and leachate for active municipal solid waste landfills. *Journal of Environmental Management*, *344*, 118443. https://doi.org/10.1016/j.jenvman.2023.118443

Lando, A. T., Nakayama, H., & Shimaoka, T. (2017). Application of portable gas detector in point and scanning method to estimate spatial distribution of methane emission in landfill. Waste Management, 59, 255–266. https://doi.org/10.1016/j.wasman.2016.10.033

Liland, KH. 2015. 4S Peak Filling – baseline estimation by iterative mean suppression. *MethodsX* 2: 135–140. https://doi.org/10.1016/j.mex.2015.02.009

Matacchiera, F, Manes, C, Beaven, RP, Rees-White, TC, Boano, F, Mønster, J, Scheutz, C. 2019. AERMOD as a Gaussian dispersion model for planning tracer gas dispersion tests for landfill methane emission quantification. *Waste Management* 87: 924–936. https://doi.org/10.1016/j.wasman.2018.02.007

Mohsen, RA, Abbassi, B. 2020. Prediction of greenhouse gas emissions from Ontario's solid waste landfills using fuzzy logic based model. *Waste Management* 102: 743–750. https://doi.org/10.1016/j.wasman.2019.11.035

Omelchenko, M. V., Vasilyeva, L. V., & Zavarzin, G. A. (1993). Psychrophilic methanotroph from tundra soil. *Current Microbiology*, *27*(5), 255–259. https://doi.org/10.1007/BF01575988

601 Park, JR., Moon, S, Ahn, YM, Kim, JY, Nam, K. 2005. Determination of Environmental Factors
602 Influencing Methane Oxidation in a Sandy Landfill Cover Soil. *Environmental Technology* 26(1): 93–
603 102. https://doi.org/10.1080/09593332608618586

604 Pipatti, R, Svardal, P. 2006. Solid waste disposal. In: Eggleston, S, Buendia, L, Miwa, K, Ngara, T.,
605 Tanabe K, editors. 2006 IPCC Guidelines for National Greenhouse Gas Inventories. Vol 5.
606 Intergovernmental Panel on Climate Change. http://www.ipcc-
607 nggip.iges.or.jp/public/2006gl/pdf/5_Volume5/V5_3_Ch3_SWDS.pdf

608 Risk, D, Omidi, A, Bourlon, E, Khaleghi, A, Perrine, G, Tarakki, N, Martino, R, Stuart, J. 2025. Active
609 face emissions: An opportunity for reducing methane emissions in global waste management
610 [preprint]. Earth ArXiv. https://eartharxiv.org/repository/view/8891/

611 Scarpelli, TR, Cusworth, DH, Duren, RM, Kim J, Heckler, J, Asner, GP, Thoma, E, Krause, MJ, Heins,
612 D, Thorneloe, S. 2024. Investigating major sources of methane emissions at US landfills.
613 *Environmental Science and Technology* 58(49): 21545–21556.
614 https://doi.org/10.1021/acs.est.4c07572

615 Scheutz, C, Fredenslund, AM, Chanton, J, Pedersen, GB, Kjeldsen, P. 2011. Mitigation of methane
616 emission from Fakse landfill using a biowindow system. *Waste Management* 31(5): 1018–1028.
617 https://doi.org/10.1016/j.wasman.2011.01.024

618 Scheutz, C., & Kjeldsen, P. (2004). Environmental Factors Influencing Attenuation of Methane and
619 Hydrochlorofluorocarbons in Landfill Cover Soils. *Journal of Environmental Quality*, *33*(1), 72–79.
620 https://doi.org/10.2134/jeq2004.7200

621 Spokas, KA, Bogner, JE. 2011. Limits and dynamics of methane oxidation in landfill cover soils. *Waste*
622 *Management* 31(5): 823–832. https://doi.org/10.1016/j.wasman.2009.12.018

623 Thompson, S, Sawyer, J, Bonam, R, Valdivia, JE. 2009. Building a better methane generation model:
624 Validating models with methane recovery rates from 35 Canadian landfills. *Waste Management* 29(7):
625 2085–2091. https://doi.org/10.1016/j.wasman.2009.02.004

626 Turner, DB. 1964. A diffusion model for an urban area. *Journal of Applied Meteorology and Climatology*
627 3(1): 83-91. https://journals.ametsoc.org/view/journals/apme/3/1/1520-
628 0450_1964_003_0083_admfau_2_0_co_2.xml

629 Vu, HL, Ng, KTW, Richter, A. 2017. Optimization of first order decay gas generation model parameters
630 for landfills located in cold semi-arid climates. *Waste Management* 69: 315–324.
631 https://doi.org/10.1016/j.wasman.2017.08.028

632 Wang, Y, Fang, M, Lou, Z, He, H, Guo, Y, Pi, X, Wang, Y, Yin, K, Fei, X. 2024. Methane emissions
633 from landfills differentially underestimated worldwide. *Nature Sustainability* 7(4): 496–507.
634 https://doi.org/10.1038/s41893-024-01307-9

635 Xu, L., Lin, X., Amen, J., Welding, K., & McDermitt, D. (2014). Impact of changes in barometric
636 pressure on landfill methane emission. *Global Biogeochemical Cycles*, *28*(7), 679–695.
637 https://doi.org/10.1002/2013GB004571

638

639

Contributions

Contributed to conception and design: DR, SF, FV

Contributed to acquisition of data: JS, RM, LC, DR

Contributed to analysis and interpretation of data: EB, DR, JS, RM, LC, EL, NB, SF, SA, FV

Drafted and/or revised the article: JS, DR, EB, RM, LC, EL, NB, SF, SA, FV

Approved the submitted version for publication: DR, EB, JS, RM, LC, EL, NB, SF, SA, FV

Acknowledgments

We thank all landfill operators who facilitated our work. We also appreciate the contributions of the skilled Environment and Climate Change Canada staff in the Pollutant Inventories and Reporting Division, Climate Research Division, and Waste Reduction and Management Division. We would like to thank Dr. Anders Fredenslund, of the Technical University of Denmark, as well as two anonymous reviewers for taking the time and effort necessary to review our manuscript. We sincerely appreciate their valuable comments and suggestions, which have helped us to improve the quality of the manuscript.

Funding information

Funding for the study was made available by Environment and Climate Change Canada through a Contribution Agreement to St. Francis Xavier University.

Competing interests

The authors declare that there are no competing financial or personal interests in relation to the work described.

Supplemental material

S1 Quantification of methane sources using mobile plume transects. This section describes the inversion approach based on the Gaussian Plume Model used to estimate methane emission rates from mobile measurements in this study.

S2 Climate category definition. This section presents our exploration of climate parameters (precipitation, aridity, temperature, and climatic regions), which led to the definition of the selected climate categories.

These 2 sections are included in a PDF document, intitled "Stuart_Canada_Landfills_Study_Elementa_Supplementary_Material.pdf"

Data accessibility statement

The data presented in this study are available at https://doi.org/10.5683/SP3/PGJX03. In this file, the landfill geolocation was removed to preserve site anonymity.

Figures

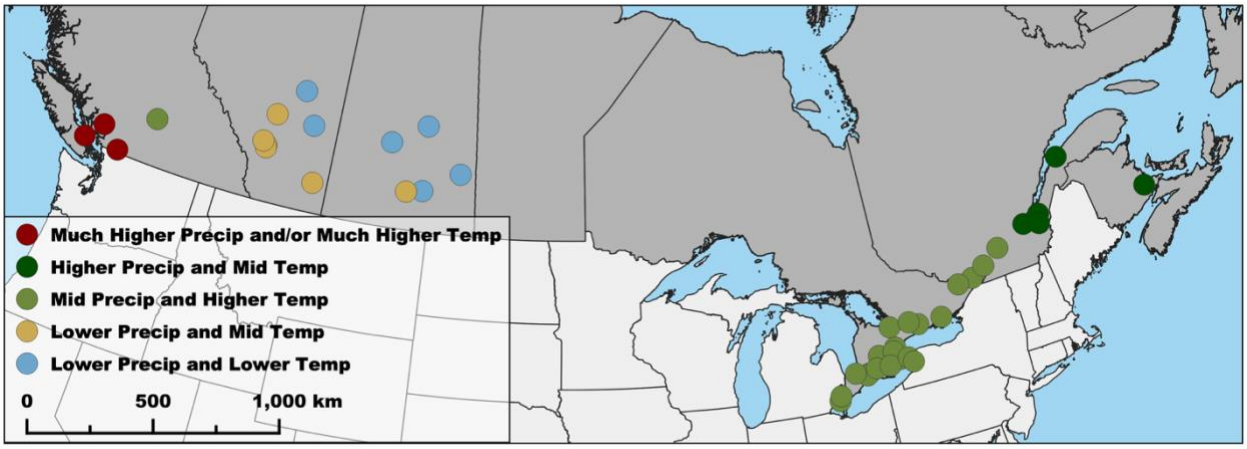

Figure 1. Locations of landfill sites.

The colors represent the climate categories based on precipitation amounts and mean temperatures from 2018 to 2022.

Alt Text: Map of southern Canada and the northern United States showing the locations of landfills included in this study. Each landfill is marked with a colored dot indicating one of five climate categories based on recent (2018–2022) precipitation and temperature conditions: much higher precipitation and/or temperature (red), higher precipitation and mid temperature (dark green), mid precipitation and higher temperature (green), lower precipitation and mid temperature (yellow), and lower precipitation and temperature (blue). Provincial and state borders are outlined for geographic reference. Canadian provinces appear in medium grey, U.S. states in light grey, and oceans and other water bodies in blue.

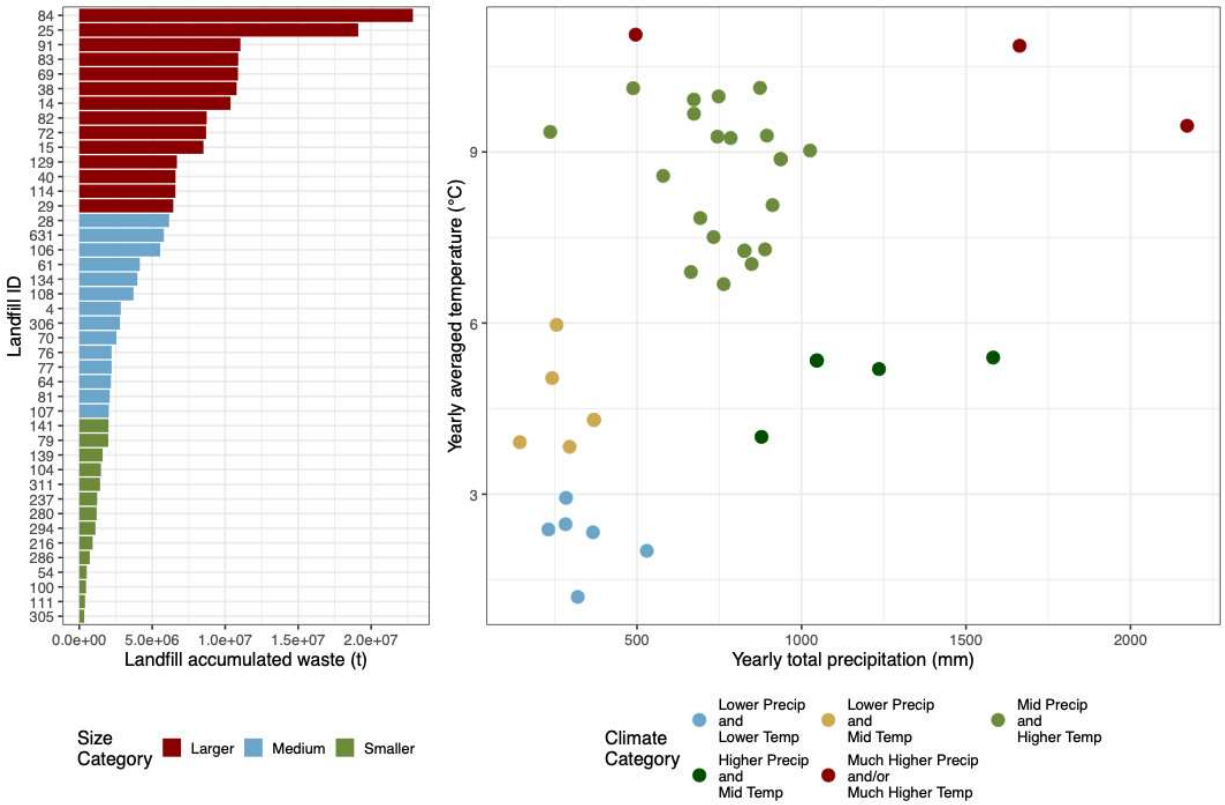

Figure 2. Landfill sizes and climate categories.

The left panel shows the distribution of landfill size, based on the accumulated waste tonnage as of 2022. Sizes were divided into 3 groups, and the colors of the bars indicate the size category of each landfill. The right panel represents the yearly average temperature (in °C) versus the yearly average precipitation amount (in mm) for each landfill. Both quantities were calculated using weather data from ECCC stations located within 50 km of each site. The colors indicate the climate clusters we used in this study.

Alt Text: Left: this bar chart ranks landfills, identified by ID number on the y axis, by their accumulated waste in tonnes. They are categorized into three groups: Larger (red), Medium (blue), Smaller (green). Right: This scatter plot maps landfills based on their precipitation (x axis, in mm) and temperature (y axis, in °C) conditions. Each landfill is marked with a colored dot indicating one of five climate categories based on recent (2018–2022) precipitation and temperature conditions: much higher precipitation and/or temperature (red), higher precipitation and mid temperature (dark green), mid precipitation and higher

temperature (green), lower precipitation and mid temperature (yellow), and lower precipitation and temperature (blue).

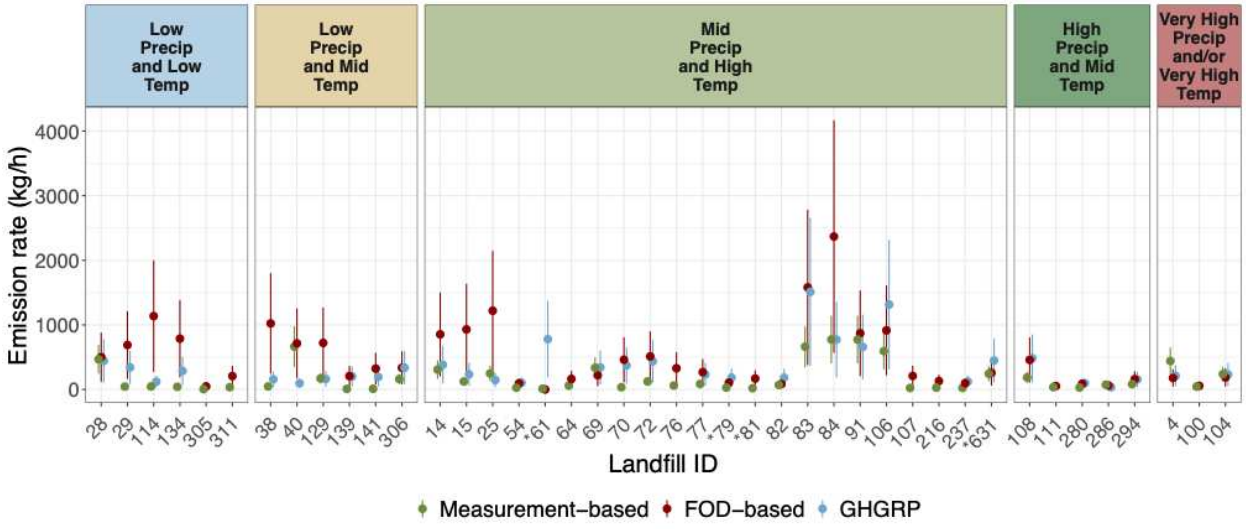

Figure 3. Bias-corrected measurement-based methane emission rate estimates, industry-reported GHGRP estimates, and ECCC FOD model estimates.

The figure shows the emission rate estimates used in this study. Bias-corrected, measurement-based estimates are shown in green, ECCC FOD-based estimates in red, and GHGRP-reported estimates in blue. The error bars represent the reported uncertainty: ±76% for the IPCC FOD modeled rates and ±47.6% for measurement-based rates. Emissions are grouped by climate category to highlight where divergences occur. Closed landfills are identified by an asterisk (*) in front of their identification number.

Alt Text: This chart compares landfill methane emission rates in kg/h (on the y axis) across five different climates using three methodologies. Measurement-based rates are displayed in green, FOD-based rates in red, and GHGRP-reported rates in blue. Landfills are grouped by climate conditions as indicated by the top strip color: lower precipitation and temperature (blue), lower precipitation and mid temperature (yellow), mid precipitation and higher temperature (green), higher precipitation and mid temperature

(dark green), and much higher precipitation and/or temperature (red). The landfill IDs are indicated on the x axis.

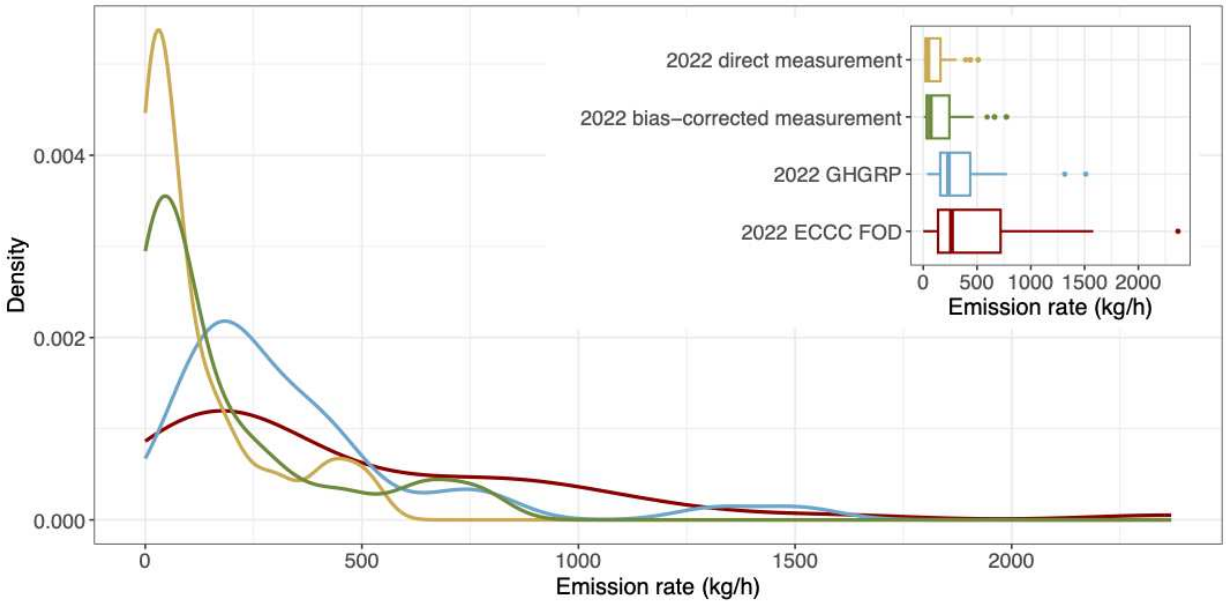

Figure 4. Density plot of landfill direct and bias-corrected measurement-based emission rate estimates, industry-reported GHGRP estimates, and ECCC FOD model estimates.

This figure highlights the difference in the distribution of each rate product. The inset illustrates how the range of each rate product compares to the others.

Alt Text: This line plot compares different methods for estimating greenhouse gas emission rates based on 2022 data. The main panel shows probability density curves of emission rates (kg/h), indicating where values most frequently occur for each method. An inset plot in the top right summarizes the distribution for each method, showing the median, interquartile range, and potential outliers. Yellow lines and boxes represent direct measurement-based rates, green indicates bias-corrected measurement-based rates, blue shows GHGRP-reported rates, and red shows FOD-modelled rates.

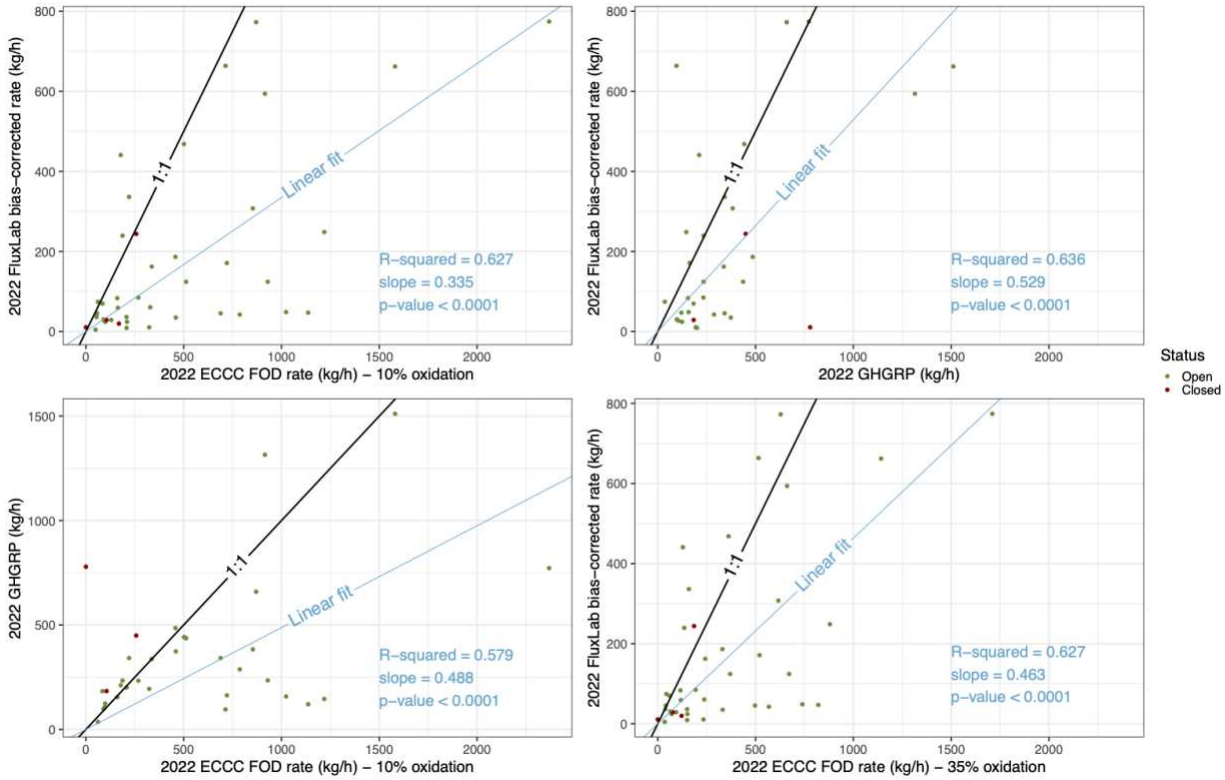

726

727 **Figure 5. Linear regressions between the measurement-based rates, the ECCC modeled rates, and**
728 **the GHGRP reported rates.**

729 Left column: Measurement-based emission rate estimates (top) and GHGRP (bottom) versus ECCC FOD
730 model estimates. Right column: Measurement-based estimates versus GHGRP (top) and versus ECCC
731 FOD model with 35% methane oxidation (bottom). Note that the reported uncertainty for the IPCC FOD
732 modeled rate, using the standard parameters, is ±76%, while the uncertainty for measurement-based
733 rates—estimated from the controlled release experiment—is 47.6%.

734 Alt Text: This figure presents four scatter plots comparing different methods for estimating methane
735 emission rates (kg/h) from landfills in 2022. Each data point is classified by landfill status: open sites are
736 shown in green and closed sites in red. In every plot, the blue line indicates the best linear fit between the
737 two methods being compared, while the black line shows the 1:1 parity line for reference.

738

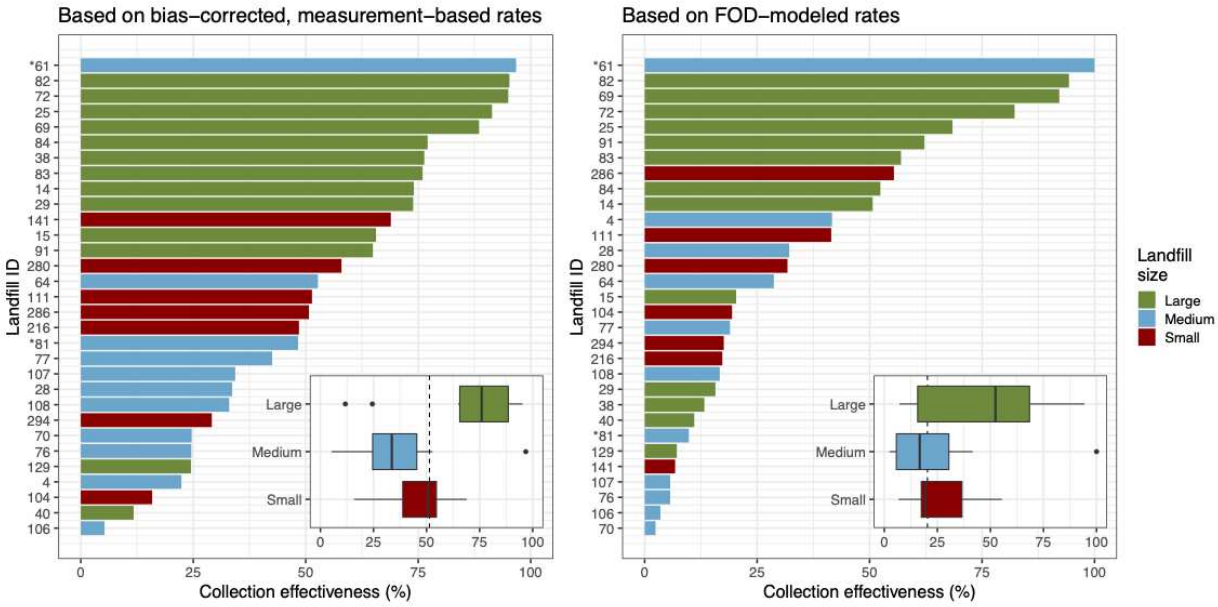

739

740 **Figure 6. Methane collection effectiveness.**

741 Collection effectiveness based on measurement-based rates (left) and ECCC FOD modeled rates with
742 10% oxidation (right), ordered by increasing collection efficiency. The insets show a box plot of the
743 effectiveness by landfill size, indicating the median, interquartile range, and potential outliers.

744 Alt Text: Two side-by-side bar charts comparing landfill gas collection effectiveness (percent on the
745 x-axis) across landfill IDs (y-axis), categorized by size: Large (green), Medium (blue), and Small (red).
746 The left chart shows effectiveness based on bias-corrected, measurement-based emission rates, and the
747 right chart shows effectiveness based on FOD-modeled emission rates. An inset in the bottom-right
748 corner of each chart contains boxplots summarizing collection effectiveness for each size category.

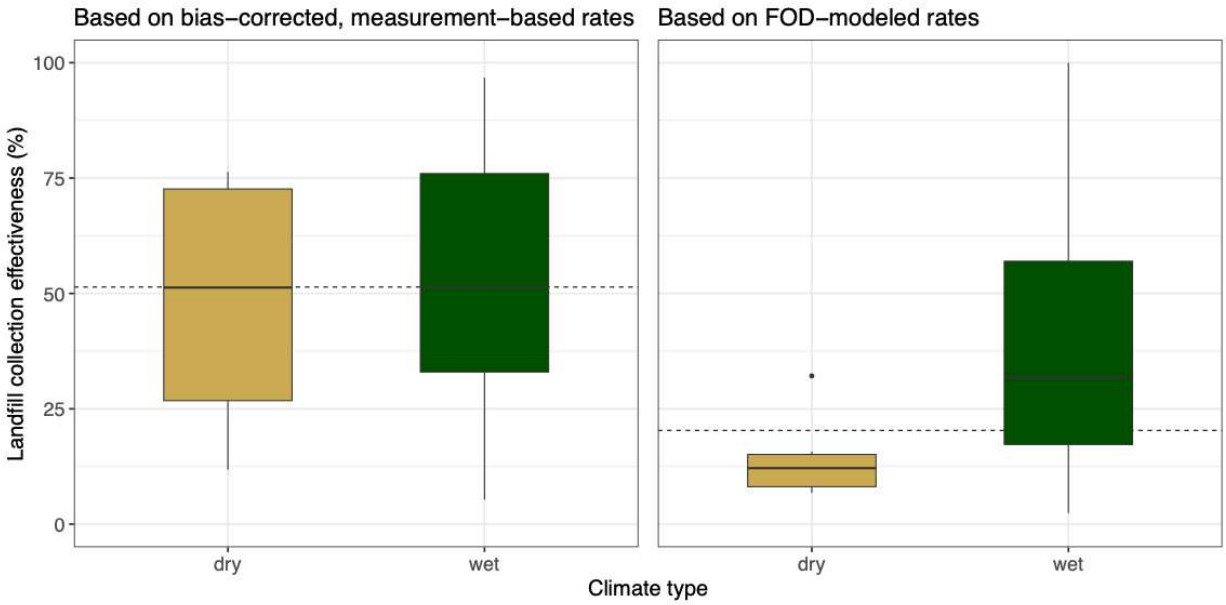

749

750 **Figure 7. Collection efficiency per type of climate, based on measurement-based rate (left) and on**
751 **ECCC FOD modeled rates (right).**

752 The "dry" climate type combines the two lowest precipitation categories, and the "wet" type includes the
753 mid, high, and highest precipitation climate categories. Efficiencies estimated using measurement-based
754 rates show no relationship with climate. In contrast, efficiencies derived from the FOD modeling reveal a
755 pronounced difference between dry and wet climates. In the box plots, the box extends from the first
756 quartile to the third quartile. The horizontal line within the box represents the median of the data set. The
757 lower whisker extends to the smallest non-outlier in the data set, and the upper whisker extends to the
758 largest non-outlier. Outliers are plotted separately as individual points.

759 Alt Text: A side-by-side comparison of two box plots showing the landfill collection effectiveness (%)
760 categorized by climate type (dry, in yellow, vs. wet, in green). The left box plot is based on bias-
761 corrected, measurement-based rates. The right box plot is based on FOD-modelled rates. A horizontal
762 dashed line indicated the overall (dry and wet) median collection effectiveness.

763

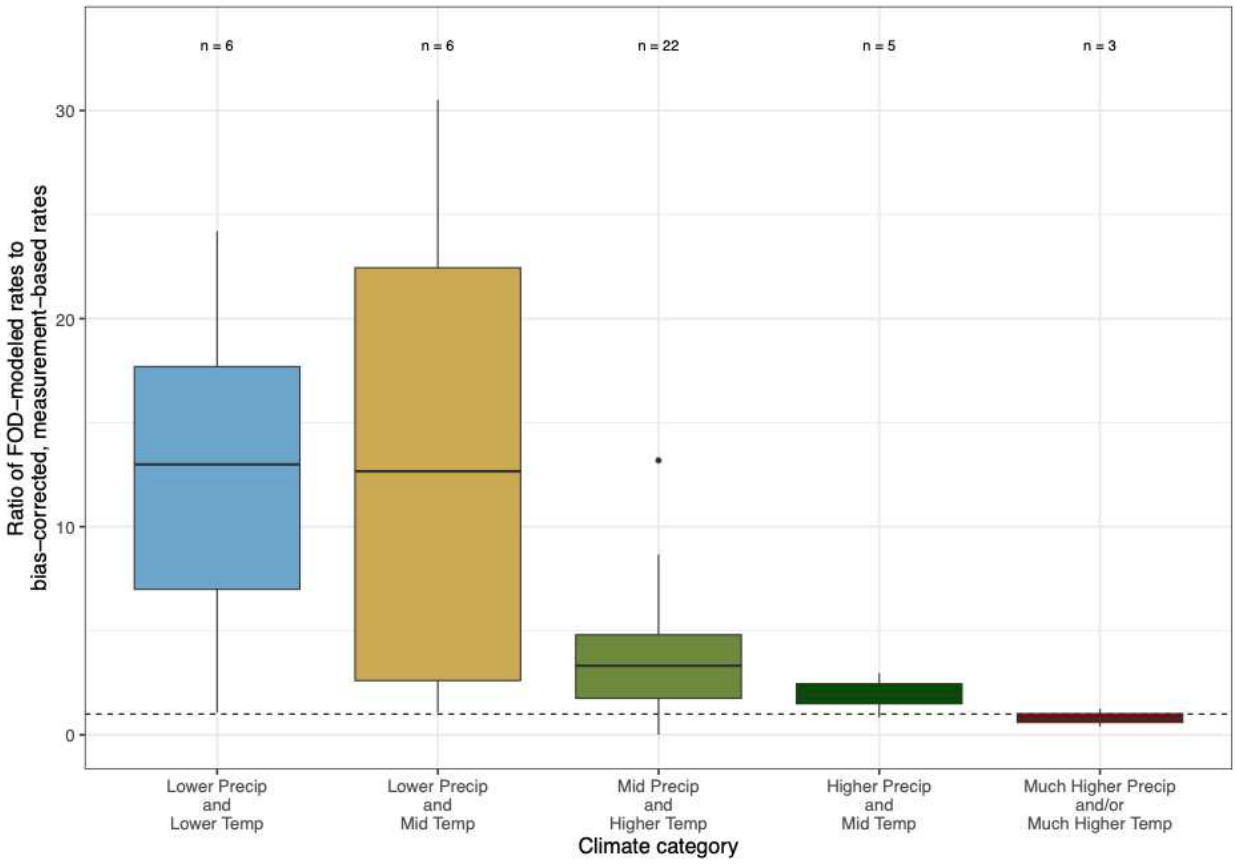

764

765 **Figure 8. Ratio of measurement-based to FOD-modeled rate estimates across climate categories.**

766 This figure highlights the amplitude of the difference between measurement-based rates and ECCC
767 modeled rates. The dashed line represents the 1:1 ratio. When boxes are above this line, ECCC rates are
768 higher than the measurement-based rates, and when ECCC rates are lower than the measurement-based
769 rates. The box extends from the first quartile to the third quartile. The horizontal line within the box
770 represents the median of the data set. The lower whisker extends to the smallest non-outlier in the data
771 set, and the upper whisker extends to the largest non-outlier. Outliers are plotted separately as individual
772 points. The numbers on top of the boxes indicate the number of landfills in each climate category.

773 Alt Text: Box plot comparing the ratio of FOD-modeled rates to bias-corrected, measurement-based rates
774 across five climate categories. Each box corresponds to a climate category coded by color: blue (lower
775 precipitation and lower temperature), yellow (lower precipitation and mid temperature), green (mid

776 precipitation and higher temperature), dark green (higher precipitation and mid temperature), and red
777 (much higher precipitation and/or much higher temperature).

778

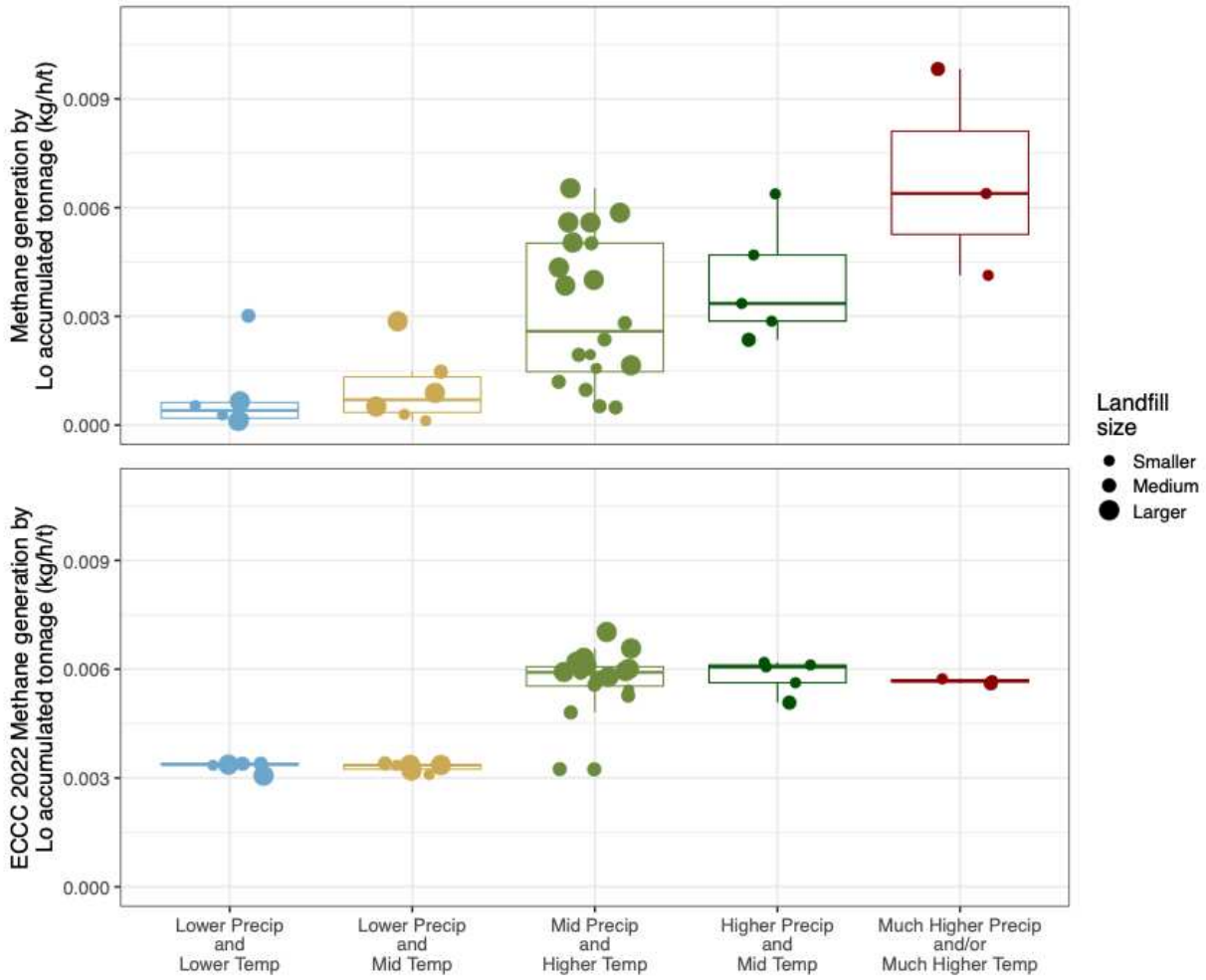

779

780 **Figure 9. Relation between methane generation per methane potential (L_0 accumulated tonnage)**
781 **and climate zone.**

782 In the top plot, the methane generation was calculated using 2022 reported collection volumes and 2022
783 measurement-based methane emissions. The 2022 methane generation rate from the ECCC FOD
784 modeling is used in the bottom plot. Each box extends from the first quartile to the third quartile. The

horizontal line within the box represents the median of the data set. The lower whisker extends to the smallest non-outlier in the data set, and the upper whisker extends to the largest non-outlier.

Alt Text: Two stacked box plots comparing methane generation (in kg/h/t; y axis) across five climate categories (x axis). Climate categories are color-coded: blue (lower precipitation and lower temperature), yellow (lower precipitation and mid temperature), green (mid precipitation and higher temperature), dark green (higher precipitation and mid temperature), and red (much higher precipitation and/or much higher temperature). Individual landfill methane generation is shown as points, with point size proportional to landfill size category (Smaller, Medium, Larger).

Tables

Table A. Bulk landfill waste decay rates (k in y^{-1}) per climate categories based on our emission rate measurement and FOD modeling.

Waste degradation depends on several factors, including moisture and temperature. Therefore, this table also presents the median annual precipitation and median annual temperature for each climate category. The median k values are reported with their second and third quartile ranges (Median [2^{nd} quartile – 3^{rd} quartile]).

Climate category	Median precipitation (mm)	Median annual temperature (°C)	Measurement-based decay rate k (y^{-1})	FOD-based decay rate k (y^{-1})
Lower Precip and Lower Temp	302	2.4	0.004 [0.002-0.006]	0.030 [0.030-0.030]
Lower Precip and Mid Temp	275	4.3	0.007 [0.003-0.014]	0.030 [0.028-0.030]
Mid Precip and Higher Temp	774	8.9	0.024 [0.013-0.046]	0.053 [0.049-0.055]
Higher Precip and Mid Temp	1046	5.3	0.032 [0.027-0.044]	0.055 [0.051-0.055]
Much Higher Precip and/or Much Higher Temp	1663	10.9	0.063 [0.052-0.081]	0.051 [0.051-0.051]

Supplementary Material

for

Canada's Landfill Methane Inventories: The Challenge of Accurate Modeled and Measurement-Based Emissions

Jordan Stuart[1], Evelise Bourlon[1], Rebecca Martino[1], Lindelwa Coyle[1], Emil Laurin[2], Nicholas Bishop[2], Susan Fraser[2], Sebastien Ars[2], Felix Vogel[2], David Risk[1,*]

[1]FluxLab, Department of Earth and Environmental Sciences, St. Francis Xavier University, Nova Scotia, Canada

[2]Environment and Climate Change Canada, Ontario, Canada

*Corresponding author: David Risk drisk@stfx.ca

Publication in Elementa—Science of the Anthropocene

October 3rd, 2025

Contents

S1 Quantification of methane sources using mobile plume transects

Gaussian plume dispersion model and assumptions

Numerous experimental field studies have been conducted to investigate the passive dispersion of non-reactive pollutants from continuous point sources, providing a foundation for the work of Sutton (1953) and Pasquill (1962). One important empirical feature is that the time-averaged concentration profiles are Gaussian in both the horizontal and vertical directions. The Pasquill-Gifford Gaussian plume model predicts concentrations from the distance to the source location, source height, source emission rate, wind speed, and dispersion coefficient. In this model, the pollutant is entirely reflected by the ground surface. Using a mathematical reference frame where the x axis is the downwind direction, the y axis the crosswind direction, and the z axis the vertical direction positive upward, the concentration χ (in µg/m3) in (x, y, z) for a continuous elevated point source located in (x_s, y_s, h) is:

$$\chi(x,y,z) = \frac{Q}{2\pi\sigma_y\sigma_z u} \times exp\left(-\frac{(y-y_s)^2}{2\sigma_y^2}\right) \times \left\{exp\left[\frac{-(z-h)^2}{2\sigma_z^2}\right] + exp\left[\frac{-(z+h)^2}{2\sigma_z^2}\right]\right\} \quad (1)$$

where σ_y and σ_z are the dispersion parameters (in m) in the crosswind and downwind direction, resp., u is the wind speed (in m/s), h is the source height (in m), and Q is the emission rate (in µg/s). The concentration χ is implicitly a function of x through the dispersion parameters. These parameters describe the horizontal and vertical spread of the plume, and their equations (known as the σ-functions) were derived by Turner (1970) by fitting the Pasquill-Gifford curves (Gifford, 1961) for open country settings. The dispersion equations are keyed to the atmospheric stability classes that express the ratio of buoyancy over mechanical turbulence. Class A corresponds to the most unstable conditions, class D to neutral conditions, and class F to the most stable conditions. The turbulence intensity increases under unstable atmospheric conditions with the development of vertical air parcel updrafts, and it is reduced under stable atmospheric conditions that suppress those vertical updrafts. There are several atmospheric stability classification schemes, and they require a variable number of meteorological variables. The Pasquill classification (Pasquill, 1961) only requires the wind speed and an estimate of the solar radiation. In this

study, we utilized a classification by Tuner (1964), where the Pasquill scheme is refined by determining an index of solar radiation using the solar elevation angle (calculated using the location and the time) and the cloud cover and ceiling height, both standard weather measurements at most weather stations. The Gaussian plume model assumes continuous emission at a constant rate and constant meteorological conditions at least over the time of transport from the source to the sensor. The effect of plume rise at the source is not considered, but the effective height can replace the source height in the equation. The Gaussian plume model should not be applied under conditions of low wind speed (< 1m/s), and the equation presented here does not account for complex terrain, or deposition and chemical reaction within the plume during travel from the source to the sensor.

Gaussian Plume Inversion

From Equation 1, the concentration from one source at one location (x, y, z) is linearly proportional to the source emission rate Q:

$$\chi(x,y,z) = Q \times \frac{\chi_{Q_1}(x,y,z)}{Q_1} = Q \times c(x,y,z) \tag{2}$$

where χ_{Q1} is the concentration for an emission rate of Q_1 and c is the concentration from a source with a unitary emission rate (1 g/s). Each concentration measurement leads to one emission rate. A joint inversion of several concentration measurements can be performed to obtain a single emission rate. In matrix form, we have to solve:

$$\chi = \begin{bmatrix} \chi_1 \\ \chi_2 \\ \vdots \\ \chi_n \end{bmatrix} = Q \times \begin{bmatrix} c_1 \\ c_2 \\ \vdots \\ c_n \end{bmatrix} \tag{3}$$

where χ is the vector of measured concentrations at locations 1 to n, Q is the emission rate, and c is the vector of concentration for a 1g/s emission rate at the same n locations. This can be generalized for multiple emitting sources. The total measured concentration is the sum of each source contribution, and equation (3) can be rewritten as

$$\chi = \begin{bmatrix} \chi_1 \\ \chi_2 \\ \vdots \\ \chi_n \end{bmatrix} = Q_1 \times \begin{bmatrix} c_{11} \\ c_{12} \\ \vdots \\ c_{1n} \end{bmatrix} + Q_2 \times \begin{bmatrix} c_{21} \\ c_{22} \\ \vdots \\ c_{2n} \end{bmatrix} + \cdots + Q_m \times \begin{bmatrix} c_{m1} \\ c_{m2} \\ \vdots \\ c_{mn} \end{bmatrix} \quad (4)$$

or

$$\chi = qC \quad (5)$$

where q is a vector of point emission rates from source 1 to m and C is an n×m matrix of concentration from source 1 to m, for a rate of 1g/s and measurement locations 1 to n.

The damping effect of the gas sensor on the methane measurement

The response of cavity ring-down instruments, such as the ones we used in our mobile survey setting, to an increase in methane varies with their flow rate and cavity size. We compared the height and area of the methane enhancements recorded by several analyzers that were sampling simultaneously, both in the laboratory (Figure S3) and in the field (Figure S1). We found that while slower instruments tend to damp peaks relative to faster ones, the areas of the peaks were similar for all instruments (Figure S2). Therefore, we used the integrated methane measurement as our data constraint in the inversion.

Inversion approach

We want to minimize the difference between χ and qC, with the constraint that all the elements of q are positive, since our input locations are sources of methane, and not sinks. We solve this problem using NonNegative Least Squares optimization:

$min_q \ \| qC - \chi \|^2$ subject to $q \geq 0$.

We use the R interface to a Fortran 77 code by Lawson and Hanson (1995), based on the algorithm described by Lawson and Hanson (1974).

Figures

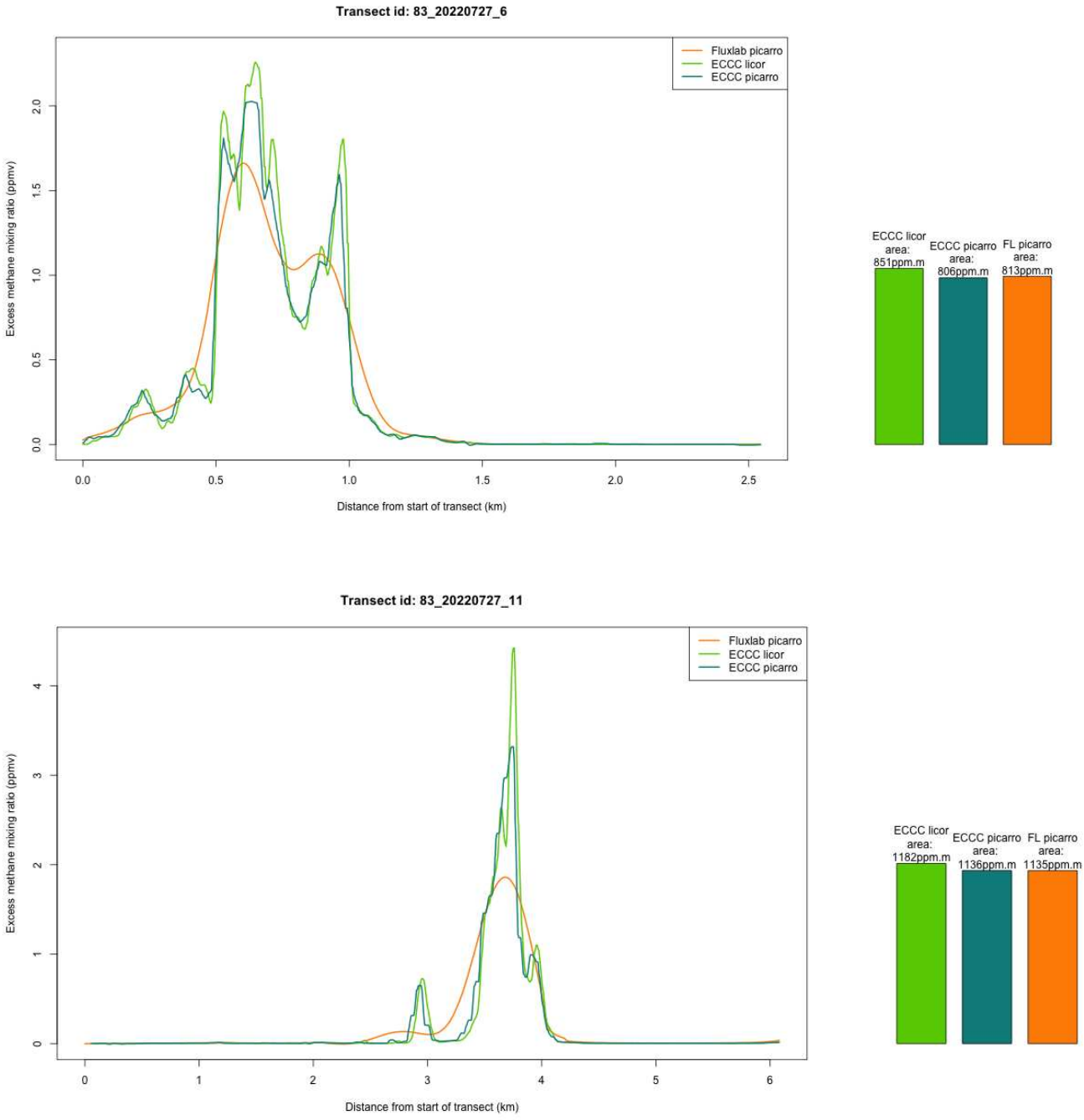

Figure S1. Two examples of field data comparison.

The plots on the left show the methane measurements, corrected for the ambient methane level, from three instruments installed in two mobile laboratories conducting simultaneous surveys at the same

location. The ECCC mobile laboratory was equipped with a Licor LI810 and a Picarro G1301. Our setting includes a Picarro 2210i, with a slower response than both ECCC instruments. The bars on the right show that, independent of the response of the instrument, the area under the curve is unchanged.

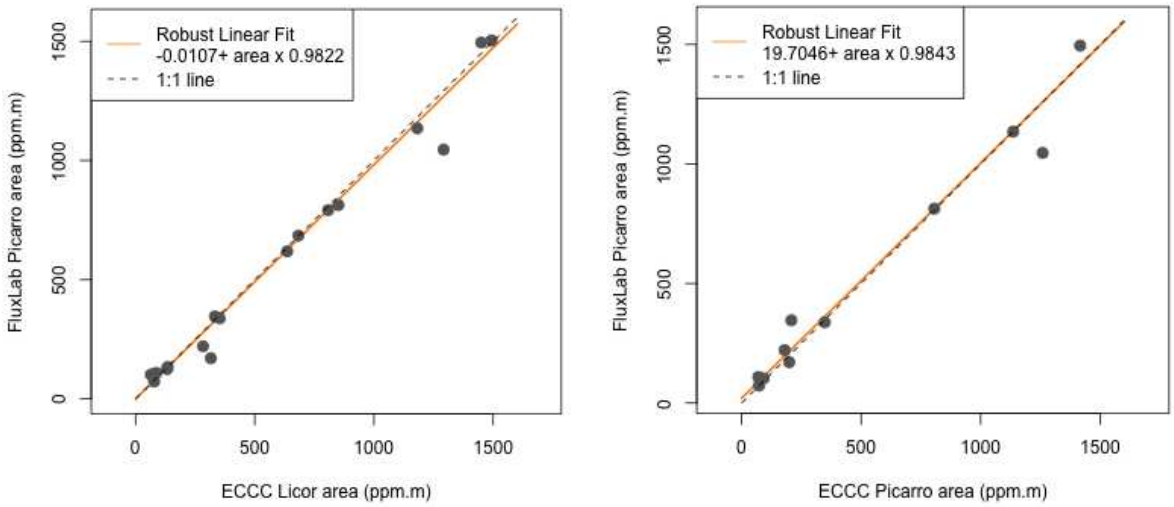

Figure S2. Comparison plots of our measured area versus each of the ECCC measured areas over multiple transects.

Left panel: ECCC Licor vs FluxLab Picarro concentration area. Right panel: ECCC Picarro vs FluxLab Picarro concentration area. Both fits are close to the 1:1 line.

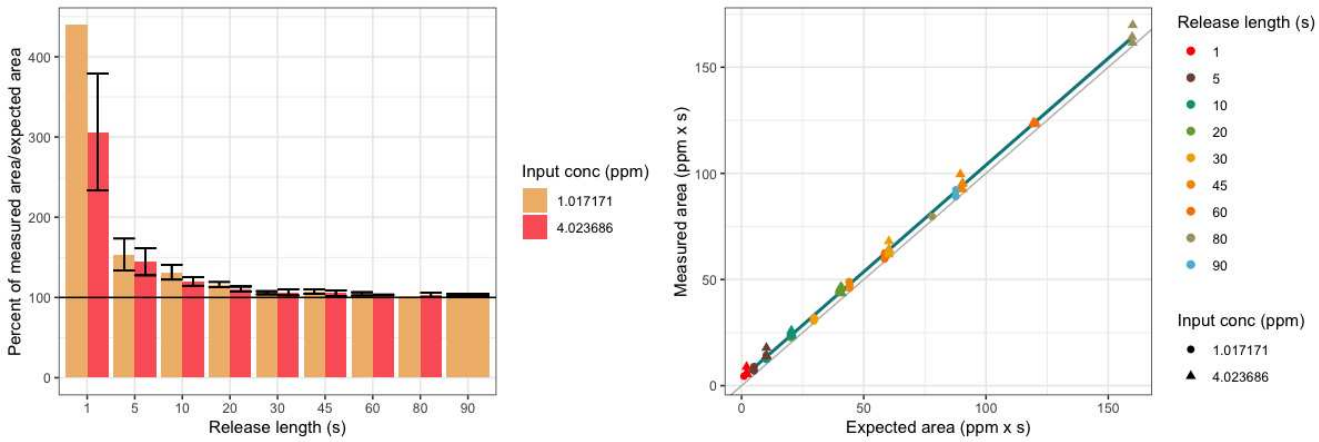

Figure S3. Illustration of the result from a laboratory measurement of our Picarro 2210i signal damping.

Timing and length of release were measured, and we used 2 methane cylinders: one at 4ppmv (~2ppmv above ambient) and one at 1ppmv (~1ppmv below ambient). Left panel: Measured area as a percentage of the expected area versus the release duration. Right panel: Measured area versus expected area. The curve integration/area is overestimated by a factor of 3 to 4 for 1s-long releases, but the overestimation is below 20% when the release is longer than 20s. The stretching of the anomaly seems to compensate for the damping of its amplitude.

References

Gifford, F. 1961. Use of Routine Meteorological Observations for Estimating Atmospheric Dispersion. Nuclear Safety, 2, 44-57.

Lawson CL, Hanson RJ. 1974. Solving Least Squares Problems. Prentice Hall, Englewood Cliffs, NJ. Lawson CL, Hanson RJ. 1995. Solving Least Squares Problems. Classics in Applied Mathematics. SIAM, Philadelphia.

Pasquill, F. 1961. The Estimation of the Dispersion of Windborne Material. Meteorology Magazine, 90, 33-40.

Pasquill, F. 1962. Atmospheric diffusion, Quarterly Journal of the Royal Meteorological Society, Vol.88(376), https://doi.org/10.1002/qj.49708837622

Sutton, OG. 1953. Micrometeorology, Quarterly Journal of the Royal Meteorological Society, Vol.79(341), https://doi.org/10.1002/qj.49707934125

Turner, DB. 1964. A Diffusion Model for an Urban Area, Journal of Applied Meteorology and Climatology, Vol.3(1), Pages 83-91, https://doi.org/10.1175/1520-0450(1964)003%3C0083:ADMFAU%3E2.0.CO;2

Turner, DB. 1970. Workbook of atmospheric dispersion estimates (Rev). U.S. Dept. of Health Education and Welfare, Public Health Service, Environmental Health Service, National Air Pollution Control Administration.

S2 Climate category definition

This section presents our exploration and definition of climate categories. As described in the main text, our initial approach used Köppen classes. One landfill falls under the BSk climate (Dry, Semi−arid steppe, Cold), three under the Cfb (Temperate, No dry season, Warm summer), one under the Dfc (Continental, No dry season, Cold summer), and the remaining 37 under the Dfb (Continental, No dry season, Warm summer).

Because three climate bins contained very few sampled sites, we instead used precipitation and temperature records from nearby ECCC airport ASOS weather stations, averaged over the five years preceding our campaign. Those are the climate categories presented in the paper.

To support our choice of climate categories, we include a map of Canada's climatic regions (Figure S4) produced by the Climate Research Branch of Environment Canada (the former name of ECCC). Our climate categories align well with those on this map, with the main difference being that the Gaspé

Peninsula (on the south shore of the St. Lawrence River in Québec) is grouped with the Atlantic Canada region.

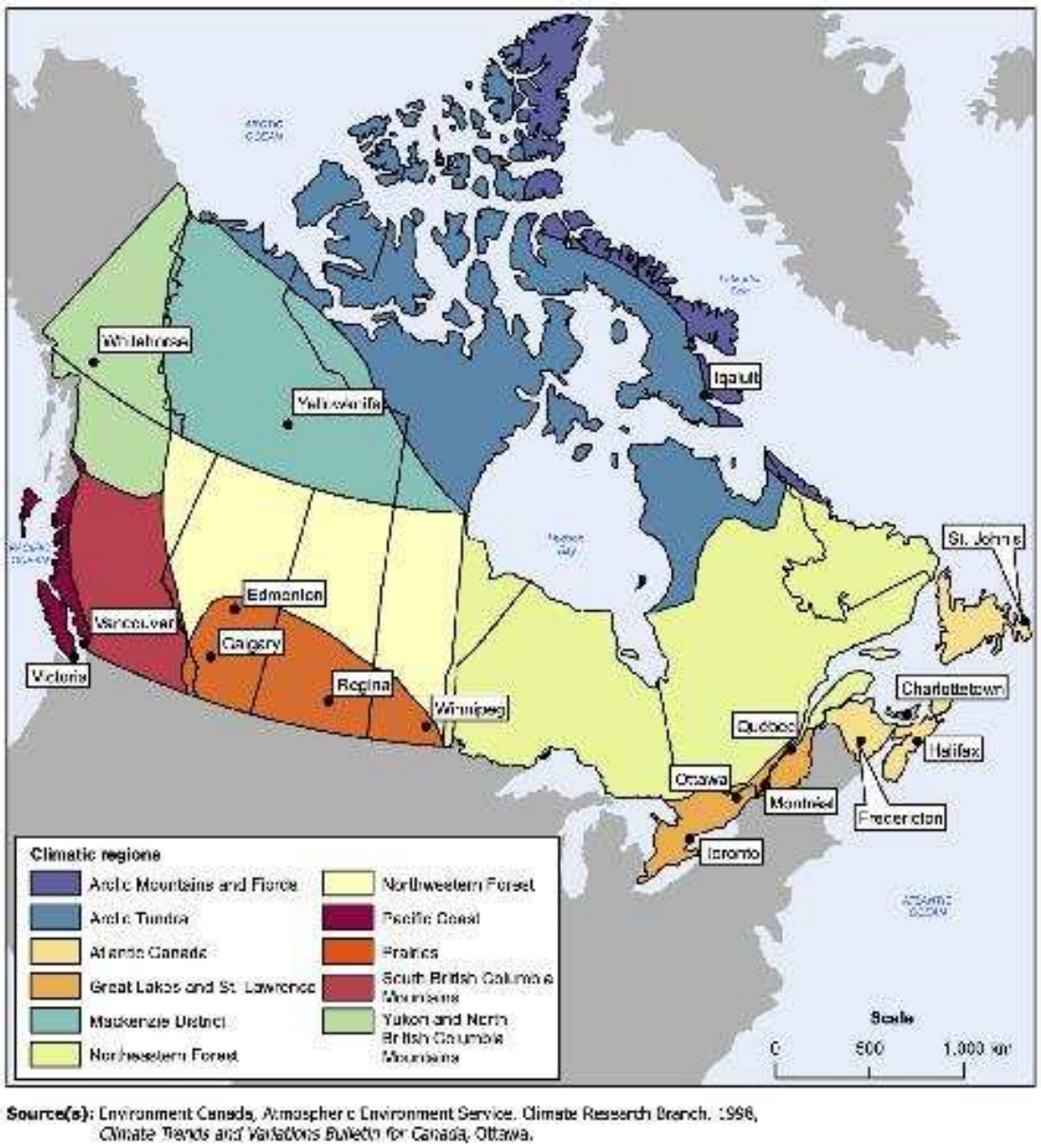

Source(s): Environment Canada, Atmospheric Environment Service. Climate Research Branch. 1998, *Climate Trends and Variations Bulletin for Canada*, Ottawa.

Figure S4. Map of the climatic regions of Canada

We also examined the ECCC climate classification based on the aridity index, defined as the ratio of precipitation to potential evapotranspiration (PET). ECCC defines two climate zones across Canada: one where PET exceeds precipitation (aridity < 1; “dry” climate) and another where PET is lower than

precipitation (aridity > 1; “wet” climate) (Figure S6). We obtained this index from the Food and Agriculture Organization of the United Nations (FAO) data website (https://data.apps.fao.org/catalog/dataset/221072ae-2090-48a1-be6f-5a88f061431a). At our selected sites, the aridity and the precipitation are roughly linearly related (Figure S5); the PET do not vary much. Adding the temperature to the precipitation or the aridity index adds another dimension to the climate classification (Figure S5).

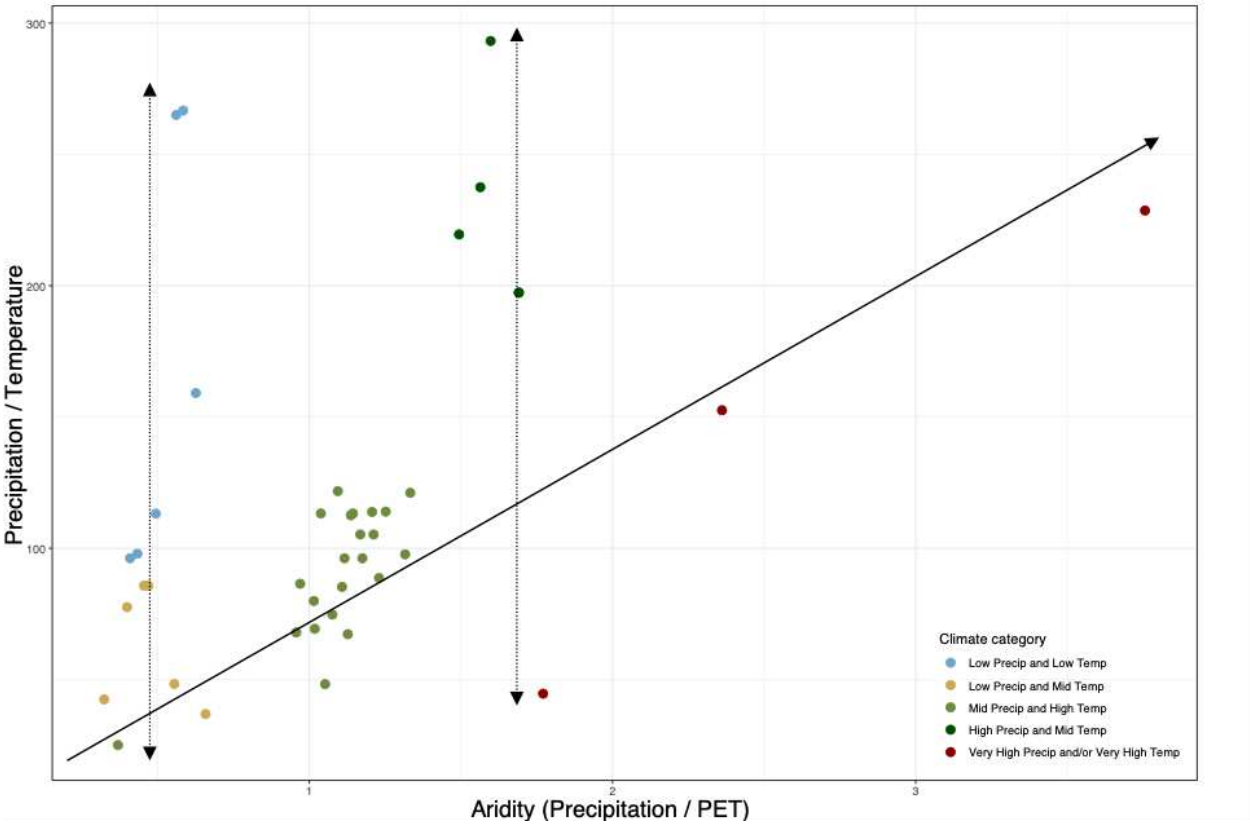

Figure S5. Precipitation over temperature versus precipitation over potential evapotranspiration. This figure shows how precipitation adds information to define climate categories.

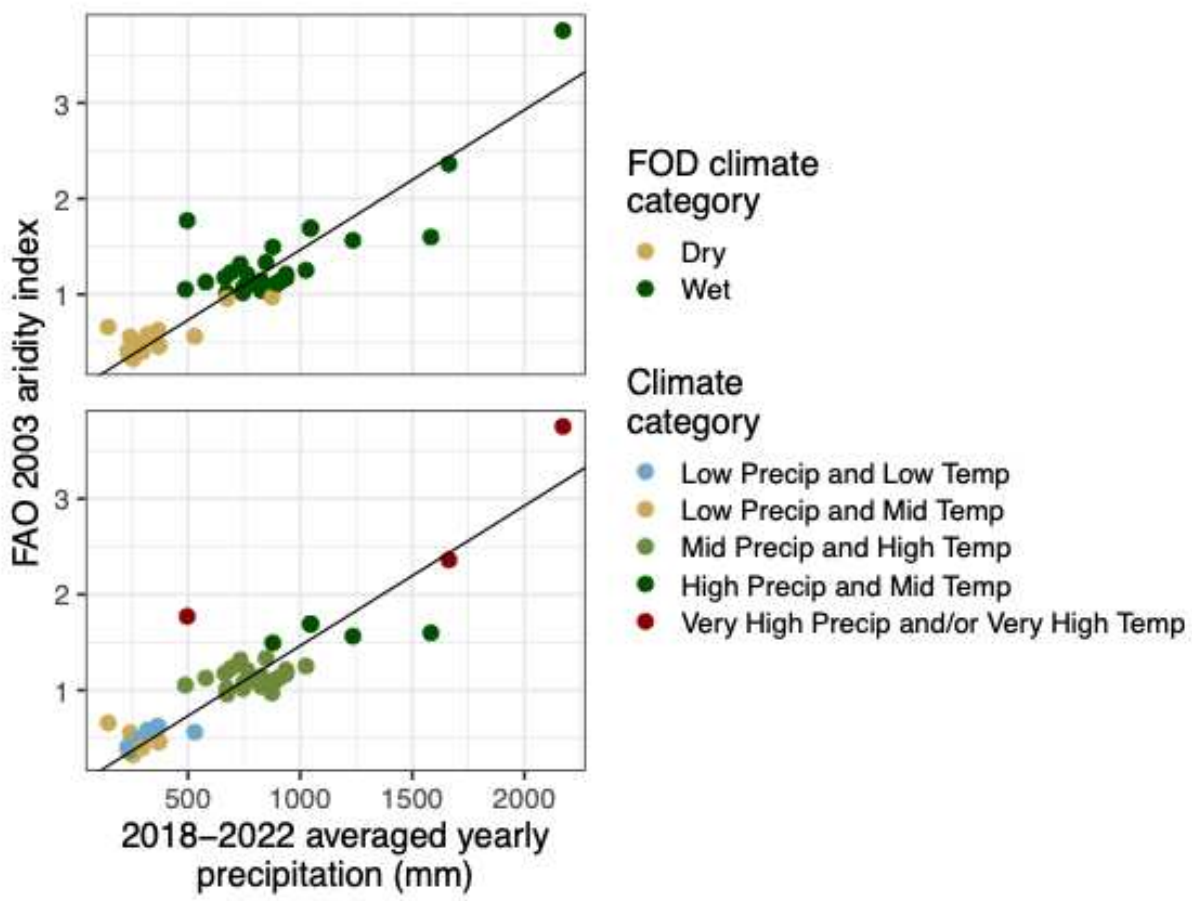

Figure S6. FAO aridity index versus yearly precipitation at the sites visited during our 2022 landfill campaign. The color used in the top plot represents the ECCC FOD climate categories, and the color used in the bottom plot are based on the climate categories used in this paper.

Our first attempt using the aridity index to define climate clusters consisted of using the aridity density plot and using the troughs between the modes as cluster limits (located in aridity = 0.72, 2.20 and 3.06; Figure S7). This resulted in 4 climate clusters, but two of them contained only one site.

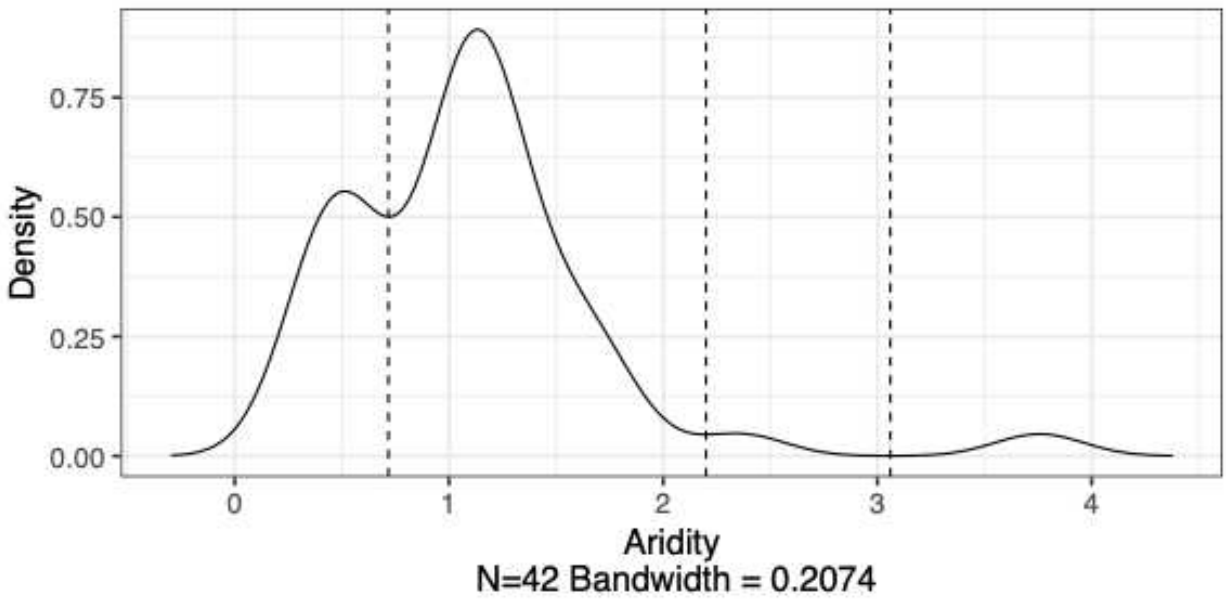

Figure S7. Density kernel estimate plot of the aridity index distribution at our selection of sites. The dashed vertical lines are located at the troughs between each mode/maximum.

We ended up defining 3 aridity-based clusters using the first trough and the slope change location of the second peak's right flank (aridity index of ~1.54), as shown in Figure S8.

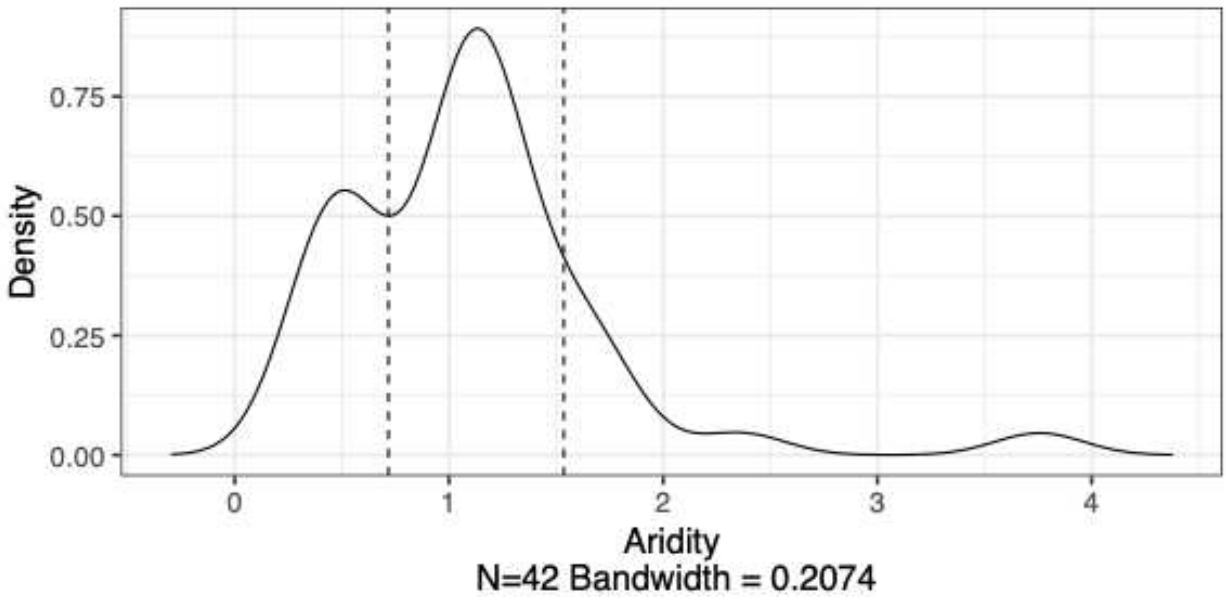

Figure S8. Density kernel estimate plot of the aridity index distribution at our selection of sites. The dashed vertical lines are located at the first trough and the change of slope on the second peak's right flank.

The low aridity index “Arid” cluster combines our “lower precipitation and lower temperature” and “lower precipitation and mid temperature” classes (sites shown in yellow and blue in the paper figures), the mid aridity index “Dry” cluster corresponds to our “mid precipitation and higher temperature” class (in light green), and the high aridity index “Humid” cluster combines our “higher precipitation and mid temperature” and “much higher precipitation and/or much higher temperature” classes (in dark green and red). We reproduced two plots from the paper using this new classification. These two figures tell the same story as the original ones:

- Figure S9, comparable to Figure 8, shows that the discrepancy between measurement-based and FOD-model emission rate estimates is more pronounced in drier climates.
- Figure S10, comparable to Figure 9, displays the bimodal variability of the FOD methane generation-over-L_0 ratio, while the measurement-based ratio shows a more gradual increase.

Both aridity-based climate clusters and precipitation and the original temperature-based clusters lead to the same conclusions in this paper. The additional clusters in the chosen classification reinforce the visual perception of the variation of the measured emissions with climate regions. These clusters are not intended for modeling purposes. We suggest that the ECCC FOD modeling would benefit from adopting an alternative aridity-based climate clustering.

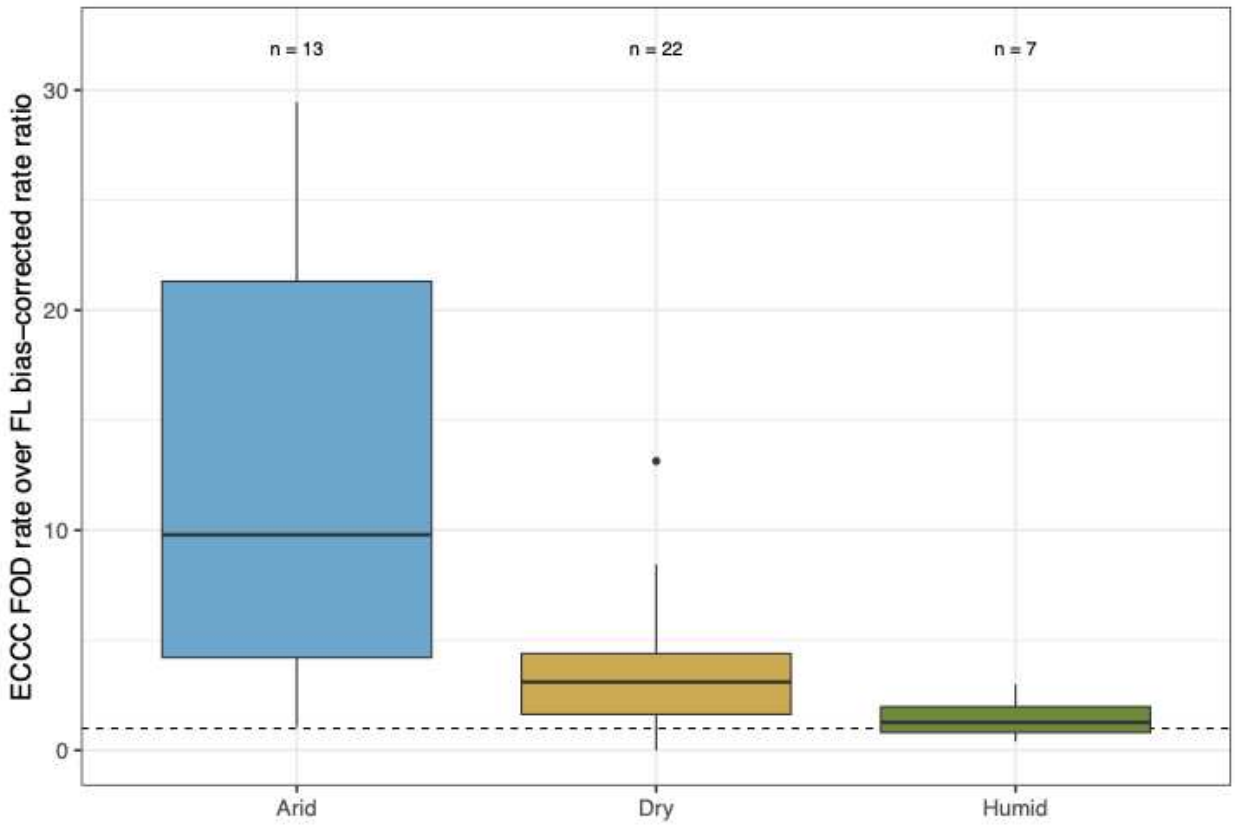

Figure S9. Ratio of measurement-based to ECCC FOD-modeled rate estimates across climate categories. Similar to Figure 8 in the paper.

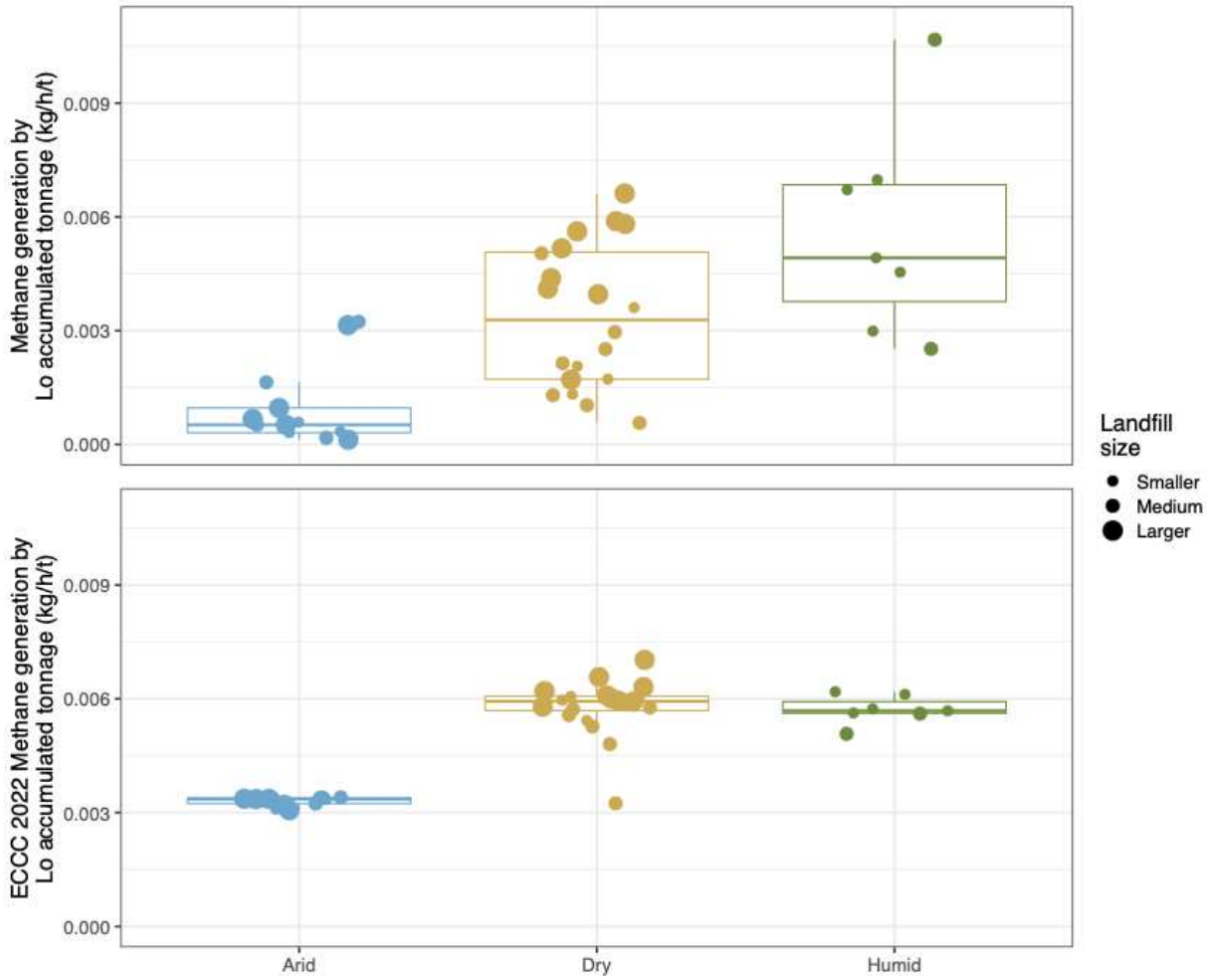

Figure S10. Relation between methane generation per methane potential (L_0 accumulated tonnage) and climate zone. Similar to Figure 9 in the paper.